Original Article

Histological Study of the Possible Therapeutic Effect of Platelet Rich Plasma on the Healing of Second Degree Skin Burn and Prevention of Scar Formation in Adult Male Albino Rat

Asmaa M. Mansour, Mona T. Sadek, Essam M. Laag, Ebtesam F. Okasha and Gehan M. Solaiman

Department of Histology and Cell Biology, Faculty of Medicine, Tanta University, Egypt

ABSTRACT

Introduction: Burn is a skin injury causing hypertrophic scars. Platelet-rich plasma (PRP) represents a therapeutic method used for wound healing.

Aim of the Work: To study the possible therapeutic effect of PRP on healing of second-degree skin burn and scar formation.

Materials and Methods: This study was done on 70 adult male albino rats, randomly divided into three main groups; I, II & III. Group I included 30 rats that were randomly divided equally into three subgroups; I-A (for blood collection), I-B (control group kept without treatment) and I-C (control group which received a single subcutaneous injection of PRP, then skin specimens were obtained after 1week and 4weeks). Group II included 20 rats in which second-degree burn was induced by heated metal rod then subdivided into 2 equal subgroups; II-A (examined after 1week) and II-B (examined after 4weeks). Group III included 20 rats in which second-degree burn was induced then the rats were immediately treated locally by one subcutaneous injection of 0.4ml of PRP and further subdivided into two equal subgroups; III-A (examined after 1week) and III-B (examined after 4weeks). Skin specimens were examined using light microscopy (H&E, toluidine blue, Mallory's trichrome, anti α SMA and CD34 immunostaining) and electron microscopy.

Morphometric study and statistical analysis were done to measure mean epidermal thickness, mean collagen area percentage and mean color intensity of α SMA and CD34 immunoreaction.

Results: In comparison to the untreated subgroups II-A and II-B, both treated subgroups III-A and III-B exhibited enhanced healing and accelerated scar maturation respectively that was more prominent after four weeks from PRP injection.

Conclusion: PRP is effective in healing and scar maturation of second-degree skin burn.

Received: 16 February 2023, **Accepted:** 25 April 2023

Key Words: Skin burn, scar, PRP.

Corresponding Author: Asmaa M. Mansour, PhD, Department of Histology and Cell Biology, Faculty of Medicine, Tanta University, Egypt, **Tel.**: +20 10 1307 8928, **E-mail:** Roaamansour2015@gmail.com

ISSN: 1110-0559, Vol. 47, No. 2

INTRODUCTION

Burn is a common household injury, especially among children. It is characterized by severe skin damage that causes death of the affected skin cells[1]. Every year, nearly 11 million of burn cases are recorded worldwide with scar formation in more than 70% of the victims and mortality reaching up to 300,000 cases[2,3].

Moreover, burn is one of the chief disability causes especially in developing countries because of pain, limited range of movement and poor cosmetic appearance causing social stigma[4]. Yet, current treatment strategies for burn are highly invasive, expensive and painful[5].

Platelet-rich plasma represents a therapeutic choice used in tissue healing enhancement and alopecia treatment due to its large content of growth factors especially platelet-derived growth factor (PDGF)[6]. These factors could accelerate wound healing and enhance the quality of the healing process[7]. PRP was used in treatment of scars following acne because it is safe, rapid, economic and less painful than other techniques[8]. According to the previous data, we designed this work in order to evaluate the possible protective PRP effect on healing of second-degree burn and prevention of scar formation.

MATERIALS AND METHODS

Experimental design

This work was done on 70 adult male albino rats aged three months. The weight of each rats ranged between 150 and 200 grams. All rats were kept in separate appropriate clean well ventilated cages under the same conditions and we fed them the same commercial laboratory diet in addition to water according to recommendations of the National Research Council of the National Academies 2011.

The experiment was performed after agreement of the Research Ethical Committee of Faculty of Medicine, Tanta University, with approval code: (33226/07/19).

Personal non-commercial use only. EJH copyright © 2024. All rights served *DOI: 10.21608/ejh.2023.193559.1858*

The animals were haphazardly divided into three main groups:

Group I: involved 30 rats that were randomly subdivided into 3 equal subgroups (10 rats each):

- Subgroup I-A (Donor group): was kept without treatment and used for collection of blood through the intracardiac route for preparation of PRP.
- Subgroup I-B (Control group): was kept without treatment and used for obtaining skin specimens for studying its normal histological structure.
- Subgroup I-C (Control group): received 0.4 ml of PRP through a single subcutaneous injection at their dorsal surface of the lower part of the back. Skin specimens were then obtained from the dorsal surface of the lower part of the back of only 5 rats of this subgroup after 1week. The remaining 5 rats were left for further 3 weeks then skin specimens were obtained from the dorsal surface of the lower part of the back (i.e. skin specimens were obtained 4 weeks after PRP injection).

Group II: included 20 rats that were anesthetized and we shaved the hair over the lower part of their back where a second-degree burn was then induced using a heated metal rod for 15 seconds[9]. This group had been equally subdivided into 2 subgroups:

- Subgroup II-A (One week after burn induction): from which skin specimens were obtained from the dorsal surface of the lower part of the back (burn site) 1 week after burn induction.
- Subgroup II-B (Four weeks after burn induction): from which skin specimens were obtained from the dorsal surface of the lower part of the back (burn site) 4 weeks after burn induction.

Group III: included 20 rats that had been anesthetized before a second-degree burn was prompted in the same site and way as in group II, then the rats were immediately subcutaneously injected in the burn site by 0.4 ml of platelet-rich plasma as a single dose[10]. This group was further equally subdivided into 2 subgroups (10 rats each):

- Subgroup III-A (Locally PRP-injected burnt group, examined one week after burn induction): from which skin specimens were obtained from the dorsal surface of the lower part of the back (burn site) 1 week after PRP injection.
- Subgroup III-B (Locally PRP-injected burnt group, examined four weeks after burn induction): from which skin specimens were obtained from the dorsal surface of the lower part of the back (burn site) 4 weeks after PRP injection.

At the appropriate time, all rats had been anesthetized by injecting sodium pentobarbital (50 mg/kg) intraperitoneal[11] then sacrificed by decapitation. The specimens were then prepared to be histologically examined by Olympus light microscope (Tokyo, Japan) that is coupled to (E-420, 10 megapixels) Olympus digital camera and by transmission electron microscope (JEOL-JEM-100 SX) at Electron Microscopy Unit, Faculty of Medicine, Tanta University. The sacrificed rats' bodies were placed in distinct packages consistent with safety measures and infection control agencies to get rid of them with the hospital biohazards.

Induction of burn injury

Rats of groups II and III had been anesthetized by 10% ketamine (90 mg/kg) and 2% xylazine (10 mg/kg) intramuscularly[12] and hair shaving was done on the dorsal surface of the lower part of the back. The thermal burn was then induced on the dorsal surface of the lower part of the back using a solid aluminum bar with a 2 cm diameter and 51 grams weight, which was previously heated for 10 minutes in boiling water at 100°C confirmed by a thermometer.

The bar was holded through its insulated handle, then placed at right angle to the shaved skin for 15 seconds provided that the thumb and the middle finger were just giving minimal support that kept the bar perpendicular to the skin and ensured that the bar was resting on the skin using only its own weight. Consequently, the pressure made on the rat's skin was equal to the weight of the bar (51 gm).

After burn induction, the rats were given analgesia by intramuscular injection of dipyrone sodium (40 mg/kg) for 3 consecutive days then maintained on oral dipyrone (200 mg/kg) administered in the feeding water[9,13].

Preparation of platelet-rich plasma (PRP)

The rats got anesthetized by 10% ketamine (90 mg/kg) in addition to 2% xylazine (10 mg/kg) through intramuscular injection[12]. Blood was collected from anesthetized donor rats directly from the heart for PRP preparation[14]. We collect 3 ml of blood from each rat using a sterilized syringe with a 23-gauge needle having 0.3 ml of 3.8% sodium citrate[15].

The blood was then put in a sterile 15 ml centrifuge (falcon) tube and the citrated blood was then centrifuged using a centrifuge at 3000 round per minute (rpm) for 7 minutes at 20°C. The buffy coat (containing leucocytes and platelets) was removed using a sterile micropipette and transported to another sterile falcon tube for a second centrifugation at 4000 rpm for 5 minutes at 20°C. A platelet pellet was formed at the tube bottom representing the part of plasma rich in platelets (platelet-rich plasma, PRP) overlayed by the plasma part poor in platelets (platelet-poor plasma, PPP) which was discarded keeping only 1ml for suspension of the platelet pellet[16].

Only 10 µl of the suspended platelet pellet was aspirated and put into a hemocytometer to count the platelets manually to validate it was PRP and that it measured nearly 5 times the normal number of platelets in the regular blood sample. The platelets number ranged from $1.4x\ 10^6$ to $2.6x\ 10^6$ /µl[17].

PRP was then activated by addition of calcium chloride at a ratio of 1:10 (0.1 ml of calcium chloride for every 1 ml of PRP). Once PRP was activated, each rat was subcutaneously injected with 0.4 ml of PRP into the burnt skin using a 26-gauge needle, within only 10 minutes after the activation.

Platelet counting

Platelets were counted using a special chamber designed for blood cells counting in a Neubauer hemocytometer that rules the chamber into 9 squares. The central square is highly ruled and subdivided into further 25 small squares. Each of the four peripheral squares is further subdivided into 16 smaller squares. The platelets appeared as bright rounded structures and were counted in the four peripheral squares, then their mean number was calculated and multiplied by the factor of the hemocytometer ($1x10^4$) to get the total number of platelets[18].

Histological and immunohistochemical studies of the skin

Skin specimens from all groups were kept in 10% formol saline for 24 hours, washed before being dehydrated through putting in rising grades of alcohol, then putting in xylol twice, 30 minutes each. The tissues were impregnated in pure soft paraffin at 60ºC for about 2 hours then embedded in hard paraffin[19]. Lastly, sections of 5 µm thickness had been cut for the following studies:

A- Histological study

1. Hematoxylin and eosin stains.
2. Mallory's trichrome stain.

B- Immunohistochemical study

1. Anti alpha smooth muscle actin (anti α SMA) immunoreaction

Anti α SMA is used to visualize smooth muscle cells located in the vascular and gut walls and the myoepithelial cells located in breast and salivary glands. It is also used to visualize pericytes of the blood capillaries and healing skin wounds[20].

Sections were deparaffinized, rehydrated before being kept in 3% hydrogen peroxide for 10-15 minutes to avoid the effect of endogenous peroxidase. Then, sections were immersed in a preheated citrate buffer solution (pH 6) with keeping heat in the microwave at 2 watts for 10-20 minutes. After that, sections were kept at room temperature for 20 minutes to cool, then washed in distilled water. Mouse monoclonal anti α SMA primary antibody (ab7817, Abcam, USA) was added at a dilution of 1:500 and totally covered the sections that were then kept overnight in a humidified chamber. Sections were then washed 4 times in phosphate buffered saline (PBS).

Secondary biotinylated goat anti-mouse antibody was supplemented to cover the sections totally for 10 minutes at 37 ºC. After that, sections were washed 4 times in PBS before streptavidin peroxidase application for 10 minutes at room temperature. Tissues were rinsed 4 times in PBS then incubated with peroxidase-compatible chromogen.

Further, sections were counterstained with hematoxylin for 30 seconds, washed, dehydrated using absolute alcohol and finally mounted.

Negative control sections had been obtained via substituting the primary antibody with buffer while human breast ductal carcinoma tissue served as the positive control. The cytoplasmic positive sites of α SMA immunoreaction appeared brown while the nuclei appeared blue[21].

2. Anti CD34 immunohistochemical stain

It reacts with CD34 antigen located in the cell membrane of dermal dendritic cells and the cytoplasm of endothelial cells, pericytes and hematopoietic cells[25]. The procedure was done using the same steps as anti α SMA immunoreaction except for that the sections had been completely covered by 50-80 µl of rabbit polyclonal CD34 primary antibody (ab185723, Abcam, USA) in the humidified chamber and left overnight then washed 4 times with PBS. Then, the sections were totally covered by 50-80 µl of the secondary biotinilated anti-mouse antibody in which they were incubated for a period of 30 minutes before the slides being washed with PBS[22,23].

C- Ultrastructural study

Preparation of semithin and ultrathin sections for transmission electron microscopic (TEM) study[24]

Specimens of the skin from all rats were divided into small pieces, 1 mm3 in size by a sharp blade and then fixed in 2.5% phosphate-buffered glutaraldehyde (pH 7.4) at 4˚C for 24 hours before being washed 3 times in the phosphate buffer (10 min each). Afterward, these skin samples were fixed in recently prepared 1% phosphate buffer osmium tetroxide (osmic acid) for about 30 min. Specimens were then soaked in phosphate buffer 3 times for 10 minutes each before being dehydrated through rising alcohol grades. Then, the skin specimens had been put into acetone (resin solvent) and epoxy resin mixture. Each specimen was then put into the tip of an individually labeled capsule which was occupied to about two-thirds of its volume with a mixture of epoxy resin and 1% of the accelerator 2, 4, 6-tri-dimethylamino methyl phenol-30.

The specimens were put in an appropriate mold which was filled with resin and allowed to be polymerized inside an oven for five days at 35˚C for 24 hours 45˚C for extra 24 hours, and lastly at 60˚C for further 3 days. Then, each block was boxed until it became very hard and then the capsule was extruded using pliers, large forceps or even by pressure on the block to be ready for sectioning.

For semithin sections, the surface of the block was trimmed into a pyramid so that the tissue in the apex had a small smooth trapezoid surface. 1 µm thick sections were cut by Leica ultracut ultramicrotome, mounted on glass slides and stained by toluidine blue to choose suitable

areas for ultrathin sectioning. On the other hand and for ultrathin sections, the block surface was retrimmed to a size appropriate for ultrathin sections using a glass knife. Sections with thickness of 75 nm were cut using LKB ultramicrotome and were carried upon 200 mesh copper grids.

The specimens had been stained twice, first stained with uranyl acetate solution for 30 minutes followed by three changes of distilled water for washing then stained with lead citrate for not more than 10 minutes, washed with distilled water and finally dried on a clean filter paper. The specimens were examined then photographed using a JEOL-JEM-100 SX electron microscope at the Electron Microscopic Unit, Faculty of Medicine, Tanta University.

D- Morphometric study and statistical analysis

Morphometric study

A software "Image J" obtained from the National Institute of Health, Bethesda, Maryland, USA was used for analysis of images. Ten diverse non-overlapping haphazardly chosen fields from every slide were microscopically examined at a magnification of 400. These specimens were measured for:

1. Mean thickness of the epidermis in H&E-stained sections.
2. Mean area percentage of collagen fibers content in Mallory's trichrome stained sections.
3. Mean color intensity of anti α SMA immunoreaction.
4. Mean color intensity of CD34 immunoreaction.

Statistical analysis

The results had been analyzed by means of one-way analysis of variance (ANOVA) then the student t-test was also used as a post-comparison test using Microsoft office Excel 2010 for Windows (Microsoft Corporation, Redmond, Washington, USA). All values had been expressed as mean ± standard deviation (SD). Changes were considered significant if the probability (*P*) values were less than 0.05 and were considered highly significant if the *P values* were less than 0.001.

RESULTS

No mortality was recorded among the rats throughout this study.

Macroscopic observation of the wounds of the experimental rats

One week after burn induction, a scab tissue was observed at the burn site of both subgroups II-A (burnt group) and III-A (locally PRP-injected burnt group). Four weeks after burn induction, obvious hair loss was observed at the burn site of subgroup II-B (burnt group), however, the skin appeared nearly normal with prominent hair growth at the burn site of subgroup III-B (locally PRP-injected burnt group) (Figure 1).

Light microscopic results

Haematoxylin and eosin-stained sections

Group I: Skin sections obtained from the control rats of subgroups I-B and I-C were similar and revealed the typical histological structure of rat skin. Epidermis was formed of stratified squamous keratinized epithelium consisting primarily of keratinocytes that were organized in four distinct layers; stratum basale, spinosum, granulosum and corneum. Stratum basale consisted of low columnar cells having large basal oval nuclei and lying on a basement membrane. Stratum spinosum was formed of polyhedral cells with central spherical nuclei while cells of stratum granulosum appeared flattened and contained basophilic keratohyalin granules. Stratum corneum (horny layer) was the most superficial non-cellular layer that consisted of acidophilic scales of keratin lamellae (Figure 2a). The dermis consisted of superficial papillary layer, consisting of loose areolar connective tissue containing blood capillaries, and deep reticular layer made up of dense irregular connective tissue containing hair follicles in addition to sebaceous glands (Figure 2b).

Group II: Subgroup II-A (One week after burn induction): This subgroup showed an area of epidermal loss that was occupied in some sections by a scab with presence of underlying inflammatory cellular infiltration and multiple large vacuoles (Figure 3). Migratory epidermal cells were observed at the edge of the injured tissues forming an epidermal tongue covering the burn site. On the other hand, migratory flattened cells were also noticed in the superficial papillary dermis at the burn edge (Figure4). The dermis showed intense inflammatory cellular infiltrate, granulation tissue with dilated blood capillaries and spindle-shaped, fibroblast-like cells (Figure5).

Subgroup II-B (Four weeks after burn induction): This subgroup revealed that the epidermis at the burn site was continuous and keratinized. Cells of stratum basale, spinosum and granulosum appeared vacuolated while stratum corneum showed overlapped keratin lamellae (Figure 6). As regards the dermis, many spindle-shaped fibroblast-like cells in addition to multiple congested blood capillaries were observed. Extravasated red blood cells together with inflammatory mononuclear cellular infiltration were noticed within the dermis in some sections (Figure 7).

Group III: Subgroup III-A (Locally PRP-injected burnt group, examined one week after burn induction): This subgroup revealed appearance of granulation tissue, formed of inflammatory cells, blood vessels and collagen, at the site of the epidermal loss (Figure 8). At the edge of the burnt tissue, the epidermal cells formed an epidermal tongue. Migratory flattened cells were noticed within the superficial dermis underlying the epidermal tongue (Figure9).

Subgroup III-B (Locally PRP-injected burnt group, examined four weeks after burn induction): Light microscopic examination of skin sections of this subgroup revealed nearly complete epidermal regeneration. The epidermis appeared continuous keratinized with apparently normal thickness resting on well-developed basement membrane. All epidermal layers appeared as those of control group with the exception of for few keratinocytes with vacuolated cytoplasm (Figures 10,11). Some blood capillaries were detected and appeared enlarged, thin-walled and septated (Figure 10). Small grouped newly formed hair follicles were also noticed in the dermis (Figure 12).

Mallory's trichrome stained sections

Group I: Mallory's trichrome-stained sections from both control subgroups I-B and I-C revealed the same normal histological appearance of collagen fibers beneath the basal lamina, in the papillary layer of dermis as fine interlacing loosely arranged fibers and in the reticular dermis as thick wavy bundles organized in different directions (Figure 13a).

Group II: Subgroup II-A (One week after burn induction): This subgroup showed thick, wavy bundles of collagen at the burn site with presence of some fused, red-stained collagen fibers (Figure 13b).

Subgroup II-B (Four weeks after burn induction): This subgroup revealed fine horizontally arranged fibers of collagen located in the superficial dermis and thicker collagen bundles within the deep dermis. Some bundles appeared parallel to each other, while others were running in different directions (Figure 13c).

Group III: Subgroup III-A (Locally PRP-injected burnt group, examined one week after burn induction): This subgroup showed thick irregularly arranged collagen bundles at the burn site in addition to some red-stained collagen fibers (Figure 13d).

Subgroup III-B (Locally PRP-injected burnt group, examined four weeks after burn induction): This subgroup showed well-organized parallel fibers of collagen in the superficial dermis, while within the reticular dermis, the collagen bundles were thick, densely packed and running in different directions (Figure 13e).

Immunohistochemical results

Anti α-SMA

Group I: Negative control skin sections revealed no immunoreaction for α-SMA (Figure 14a). α-SMA immunostained skin sections from both subgroups I-B and I-C were similar and revealed a positive brownish cytoplasmic reaction in the pericytes (Figure 14b).

Group II: Subgroup II-A (One week after burn induction): α-SMA immunostained skin sections from this subgroup showed apparently strong positive cytoplasmic reaction in the dermal myofibroblasts in addition to the pericytes (Figure 14c).

Subgroup II-B: (Four weeks after burn induction): This subgroup revealed apparently moderate positive cytoplasmic reaction in the dermal myofibroblasts and an intense positive reaction in the pericytes of the newly formed blood capillaries (Figure 14d).

Group III: Subgroup III-A (Locally PRP-injected burnt group, examined one week after burn induction): This subgroup exhibited apparently strong positive cytoplasmic reaction for α-SMA in the dermal myofibroblasts as well as in the pericytes (Figure 14e).

Subgroup III-B (Locally PRP-injected burnt group, examined four weeks after burn induction): This subgroup showed apparently strong positive reaction in the pericytes of the newly formed blood capillaries within the dermis and in the perifollicular dermal sheath (Figure 14f).

Anti-CD34

Control group: Negative control sections revealed no immunoreaction for CD34 (Figure 15a) while CD34 immunostained skin sections from both control subgroups I-B and I-C were similar and showed a localized positive membranous reaction in some dermal spindle-shaped (dendritic) cells (Figure 15b).

Group II: Subgroup II-A (One week after burn induction): This subgroup revealed apparently intense positive reaction for CD34 in both dermal capillary endothelial cell cytoplasm and the cell membranes of many dermal spindle-shaped (dendritic) cells (Figure 15c).

Subgroup II-B (Four weeks after burn induction): This subgroup exhibited apparently moderate positive reaction for CD34 in the cell membranes of some dermal spindle-shaped (dendritic) cells surrounding the healing dermis (peri-cicatritial area). However, no dendritic cells were detected in the healed areas (Figure 15d).

Group III: Subgroup III-A (Locally PRP-injected burnt group, examined one week after burn induction): Skin sections of this subgroup revealed apparently intense positive expression of CD34 in the membrane of dermal spindle-shaped (dendritic) cells and in the capillary endothelial cells cytoplasm (Figure 15e).

Subgroup III-B (Locally PRP-injected burnt group, examined four weeks after burn induction): This subgroup showed apparently moderate positive reaction in the cell membrane of dermal spindle-shaped (dendritic) cells located in the healing dermis (Figure 15f).

Electron microscopic results

Group I: Electron microscopic examination of skin ultra-thin sections obtained from both control subgroups I-B and I-C were similar and revealed that the epidermis consisted of keratinocytes, organized in four layers; stratum basale, spinosum, granulosum and corneum. Stratum basale consisted of low columnar cells resting on thin continuous basement membrane and attached to it with multiple hemidesmosomes. The cells contained oval

euchromatic basal nuclei with prominent nucleoli as well as free ribosomes and mitochondria together with few tonofilaments in their cytoplasm (Figure 16a).

Beside stratum basale, cells of stratum spinosum appeared polyhedral having oval to rounded euchromatic nuclei, prominent nucleoli as well as free ribosomes, mitochondria and excess amount of tonofibrils of intermediate keratin filaments in their cytoplasm. They appeared attached together by multiple desmosomes (Figure 16b). Cells of stratum granulosum appeared flattened with elongated nuclei. Their cytoplasm showed electron dense variable-sized keratohyalin granules and tonofilaments aggregates. Stratum corneum, the most superficial layer was formed of regularly arranged homogenous lamellae of keratin filaments (Figure 16c).

Group II: Subgroup II-A (One week after burn induction): This subgroup revealed presence of migratory epidermal tongue in which some cells of the stratum basale appeared shrunken with dense cytoplasm. Some melanocytes with multiple melanosomes were observed in between stratum basale cells. The desmosomal junctions between stratum spinosum cells were interrupted with wide intercellular spaces in between (Figure 17).

Subgroup II-B (Four weeks after burn induction): This subgroup showed stratum basale cells with flattened nuclei resting on ill-defined basement membrane (Figure 18a). In addition, wide intercellular spaces in between the keratinocytes were observed (Figure 18a). Cells of stratum spinosum appeared vacuolated (Figure 18b), some cells revealed shrunken nuclei (Figure 18b). Cells of stratum granulosum revealed their characteristic electron-dense keratohyalin granules. Keratin lamellae of the stratum corneum appeared thick, loosely packed, irregular, disorganized and poorly aligned (Figure 18c).

Group III: Subgroup III-A (Locally PRP-injected burnt group, examined one week after burn induction): This subgroup showed an epidermal tongue formed of cells of stratum basale with many melanosomes (Figure 19a), stratum spinosum cells with many cytoplasmic tonofilaments (Figure 19b) and flattened stratum granulosum cells with their characteristic keratohyalin granules (Figures 19b,19c).

Subgroup III-B (Locally PRP-injected burnt group, examined four weeks after burn induction): This subgroup showed widely separated columnar stratum basale cells having oval basal nuclei. A Langerhans cell with irregular intended nucleus and multiple lysosomes was also seen among cells of the basale layer (Figure 20a). Cells of stratum spinosum appeared polyhedral having central rounded nuclei and prominent nucleoli. Many intact intercellular desmosomal junctions were observed. Stratum granulosum layer showed flattened cells containing characteristic keratohyalin granules (Figure 20b).

Morphometric study and statistical analysis results

Mean epidermal thickness in µm (Table 1, Figure 21)

Statistical analysis of the mean epidermal thickness in subgroup II-B (139.8 ± 24.9) exhibited a highly significant increase (*P value* < 0.001) as compared to the control group (72.4 ± 9.5). Whereas the mean epidermal thickness in subgroup III-B (72.9 ± 24.9) showed a non-significant difference (*P value* > 0.05) from the control group and a highly significant decrease (*P value* < 0.001) when compared to subgroup II-B.

Mean area percentage of collagen fibers (Table 2, Figure 22)

On one hand, the mean area percentage of the collagen fibers of subgroup II-A (14.6 ± 2.5) and subgroup III-A (17.3 ± 9.9) revealed a highly significant diminution (*P value* < 0.001) when compared to the control group (36.3 ± 8.7) and a non-significant difference (*P value* > 0.05) as compared to each other.

On the other hand, the mean area percentage of collagen fibers of subgroup II-B (46.9 ± 8.2) showed a significant increase (*P value* < 0.05) when compared to the control group. Meanwhile, subgroup III-B (59.7 ± 15.7) exhibited a highly significant increase (*P value* < 0.001) when compared to the control group, subgroup II-B and also subgroup III-A.

Color intensity of anti α SMA immunoreaction (Table 3, Figure 23)

The mean color intensity of anti α-SMA immunoreaction in subgroup II-A (52.1 ± 8.9) and subgroup II-B (44.4 ± 10.3) showed a highly significant increment (*P value* < 0.001) as compared to the control group (10.8 ± 3.3). Moreover, subgroup II-B revealed a significant decrease in the color intensity (*P value* < 0.05) in respect to subgroup II-A.

On the other hand, subgroup III-A (23 ± 8.2) showed a highly significant increase in its color intensity (*P value* < 0.001) while subgroup III-B (12 ± 6.8) showed a non-significant difference (*P value* > 0.05) when both compared to the control group.

In addition, subgroups III-A and III-B showed a highly significant diminution in their anti α SMA color intensity in respect to subgroups II-A and II-B respectively. Meanwhile, subgroup III-B revealed a highly significant decrement in its color intensity as compared to subgroup III-A.

Color intensity of CD34 immunoreaction (Table 4, Figure 24)

The mean color intensity of anti CD34 immunoreaction in subgroup II-A (54.1 ± 12.7) exhibited a highly significant increment (*P value* < 0.001) as compared with the control group (34.9 ± 9.5). Subgroup II-B (6.6 ± 4.2) revealed a highly significant diminution (*P value* < 0.001) in its color intensity when compared to both control group and subgroup II-A.

Meanwhile, subgroup III-A (56.6 ± 8.4) revealed a highly significant increment in anti CD34 color intensity as compared with the control group and a non-significant difference when compared to the corresponding untreated subgroup II-A. On the other hand, subgroup III-B (32.2 ± 14.2) revealed a non-significant difference from the control group and a highly significant decrease in its color intensity as compared to subgroup III-A and the corresponding untreated subgroup II-B.

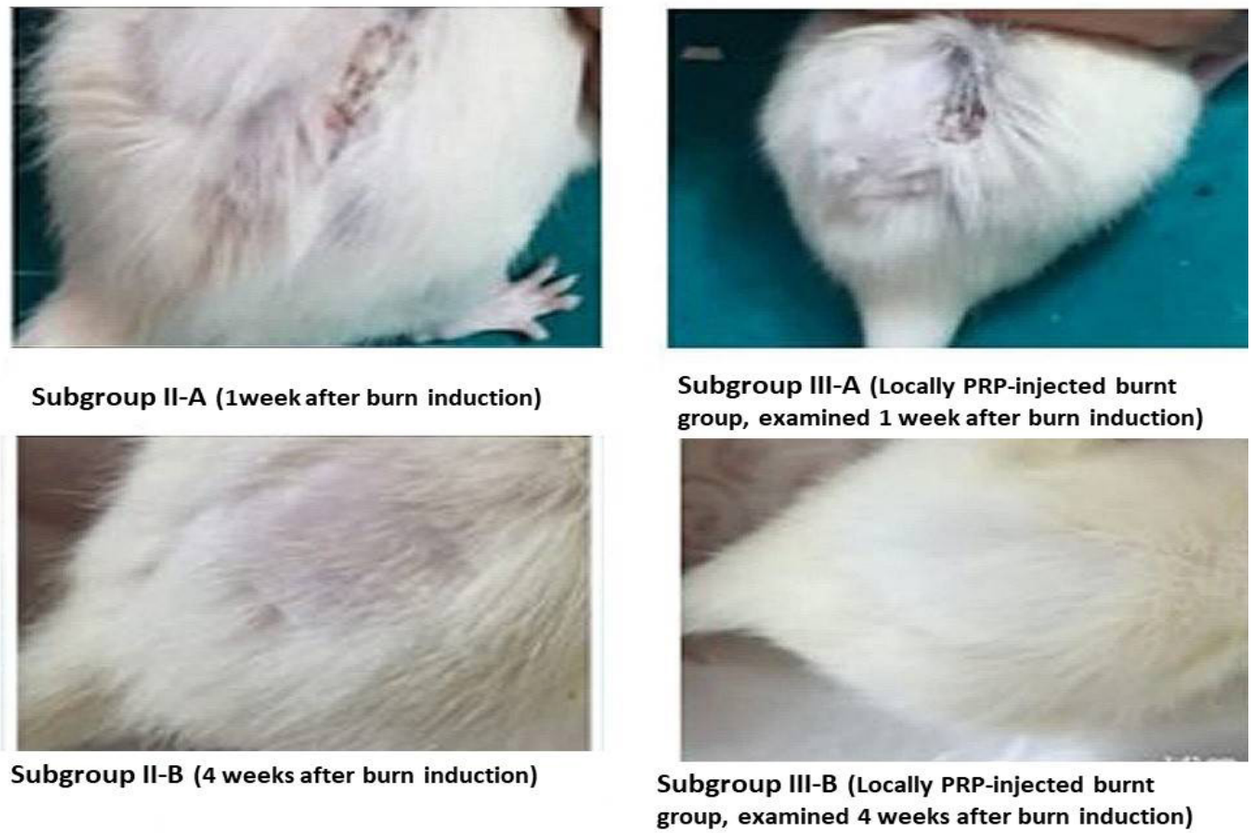

Fig. 1: Macroscopic pictures of the wounds of the experimental rats showing: A scab tissue at the burn site of both subgroups II-A (burnt group, 1 week after burn induction) and III-A (locally PRP-injected burnt group, 1 week after burn induction and PRP injection). Four weeks after burn induction, obvious hair loss is observed at the burn site of subgroup II-B (burnt group), however, the skin appears nearly normal with prominent hair growth at the burn site of subgroup III-B (locally PRP-injected burnt group).

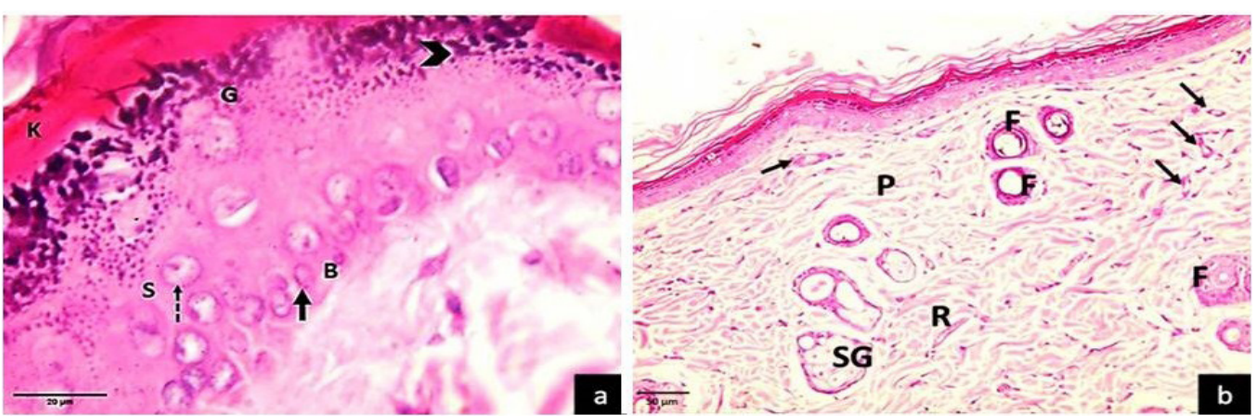

Fig. 2: Photomicrographs of sections of the control group showing: (a) The epidermis is formed of stratified squamous keratinized epithelium consisting mainly of four layers of keratinocytes. Stratum basale (B) consists of low columnar cells having large oval basal nuclei (arrow). Stratum spinosum (S) is formed of polyhedral cells containing central spherical nuclei and prominent nucleoli (dashed arrow). Stratum granulosum (G) appears as flattened cells containing basophilic granules (arrowhead). Stratum corneum (horny layer) is formed of acidophilic keratin lamellae (K). (H&E, X 1000, scale bar = 20) (b) The dermis is formed of; superficial papillary dermis (P), having blood capillaries (thin arrows) and deep reticular layer (R) containing hair follicles (F) and sebaceous glands (SG). (H&E, X 200, scale bar = 50µm)

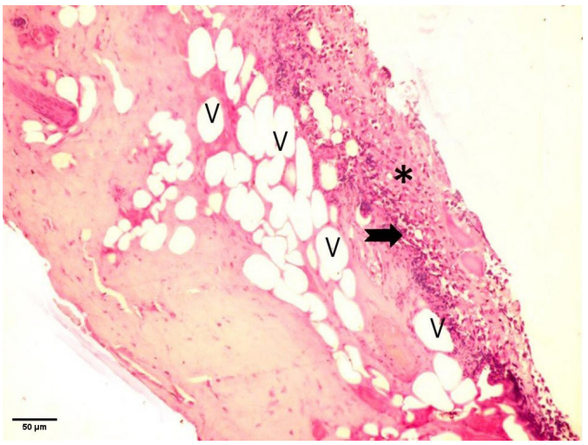

Fig. 3: A photomicrograph of a section in the skin of subgroup II-A showing an area of epidermal loss occupied by a scab (asterisk) with underlying inflammatory cellular infiltrate (notched arrow). Multiple large vacuoles (V) are also observed. (H&E, X 200, scale bar = 50µm)

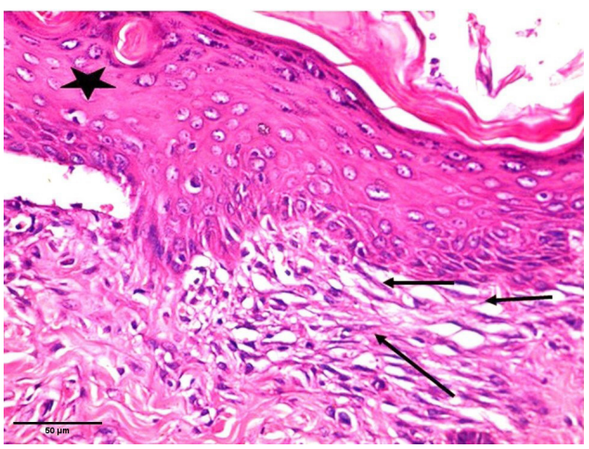

Fig. 4: A photomicrograph of a section in the skin of subgroup II-A showing the migratory epidermal cells of the epidermal tongue (star) at the edge of the injury site. Migratory flattened cells (arrow) in the superficial papillary dermis at the burn edge are also noticed. (H&E, X 400, scale bar = 50µm)

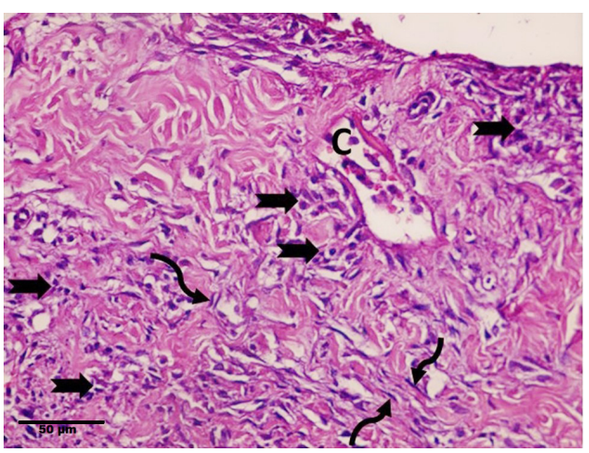

Fig. 5: A photomicrograph of a section in the skin of subgroup II-A showing granulation tissue with many fibroblast-like cells (wavy arrow), intense inflammatory cellular infiltrate (notched arrow) and a dilated blood capillary (C). (H&E, X 400, scale bar = 50µm)

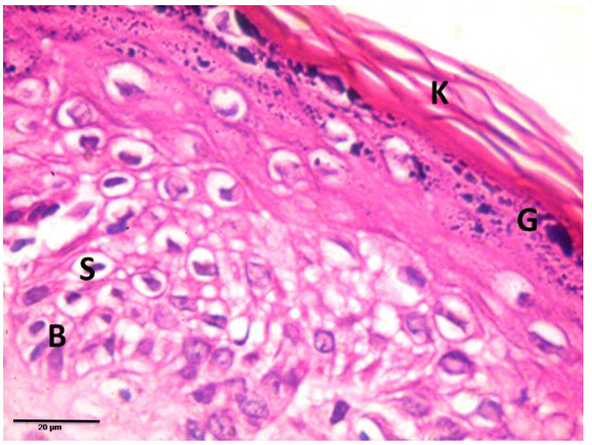

Fig. 6: A photomicrograph of a section in the skin of group II-B showing continuous and keratinized epidermis at the site of burn with most of the keratinocytes of stratum basale (B), spinosum (S) and granulosum (G) revealing vacuolated cytoplasm. Notice the overlapping keratin lamellae (K) in stratum corneum. (H&E, X 1000, scale bar = 20µm)

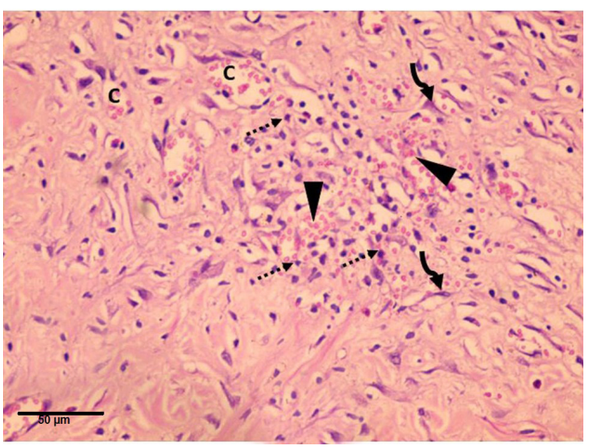

Fig. 7: A photomicrograph of a section in the skin of subgroup II-B showing mononuclear cellular infiltration (dashed arrow) and extravasated red blood cells (arrowhead) within the dermis. Notice the presence of multiple congested blood capillaries (C) and many spindle-shaped fibroblast-like cells (wavy arrow). (H&E, X 400, scale bar = 50µm)

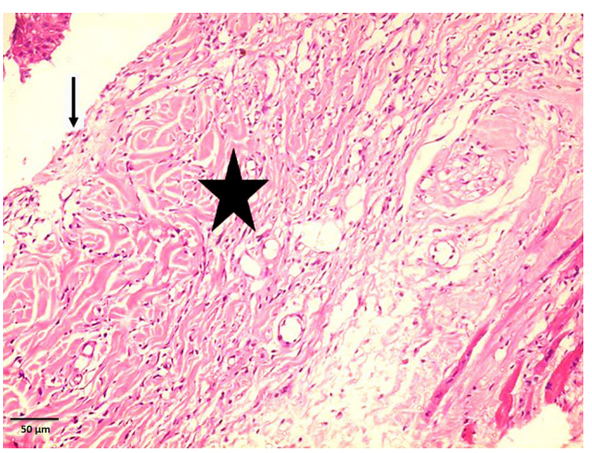

Fig. 8: A photomicrograph of a section in the skin of subgroup III-A showing area of epidermal loss (arrow) with presence of granulation tissue (star) formed of inflammatory cells, blood vessels and collagen. (H&E, X 200, scale bar = 50µm)

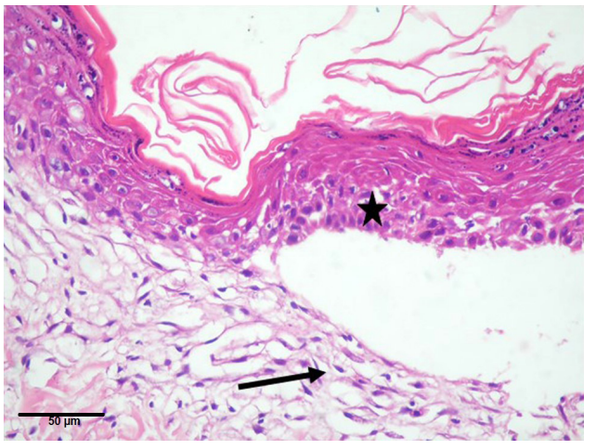

Fig. 9: A photomicrograph of a section in the skin of subgroup III-A showing an epidermal tongue (star) formed of epidermal cells at the edge of the burn site. Migratory flattened cells (arrow) are present in the superficial dermis underlying the epidermal tongue. (H&E, X 400, scale bar = 50µm)

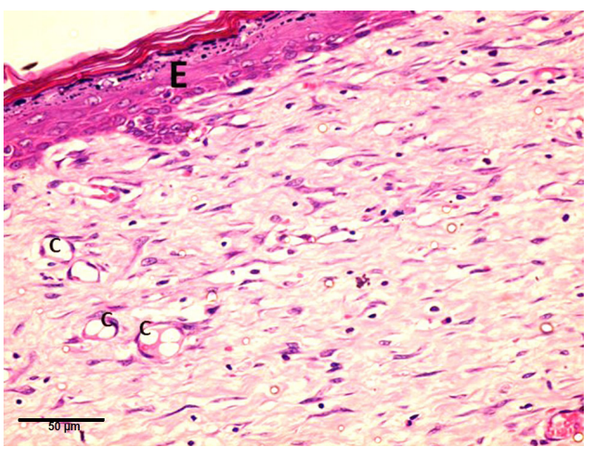

Fig. 10: A photomicrograph of a section in the skin of subgroup III-B showing apparently normal epidermal layers (E). Notice the blood capillaries (C) are enlarged, thin walled and septated. (H&E, X 400, scale bar = 50µm)

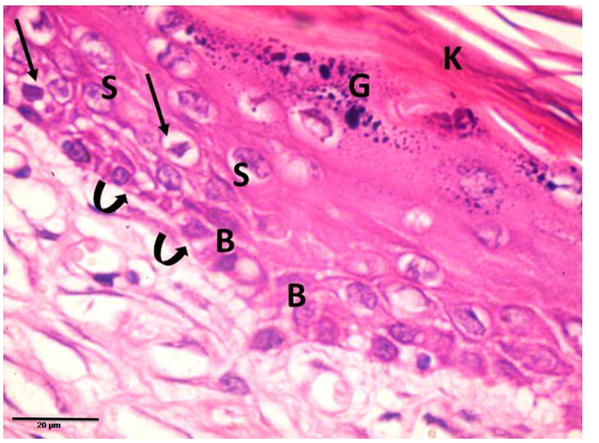

Fig. 11: A photomicrograph of a section in the skin of subgroup III-B showing apparently normal epidermal layers. Cells of stratum basale (B) have oval basal nuclei and rest on well-developed basement membrane (curved arrow). Cells of stratum spinosum (S) are polyhedral in shape having central rounded nuclei. Stratum granulosum cells (G) show their characteristic basophilic granules. Keratin lamella (K) are also present. Notice few keratinocytes (arrow) with vacuolated cytoplasm. (H&E, X 1000, scale bar = 20µm)

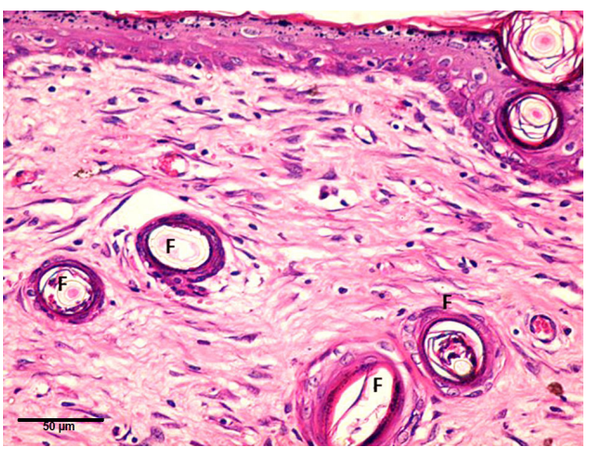

Fig. 12: A photomicrograph of a section in the skin of subgroup III-B showing small grouped newly formed hair follicles (F) in the dermis. (H&E, X 400, scale bar = 50µm)

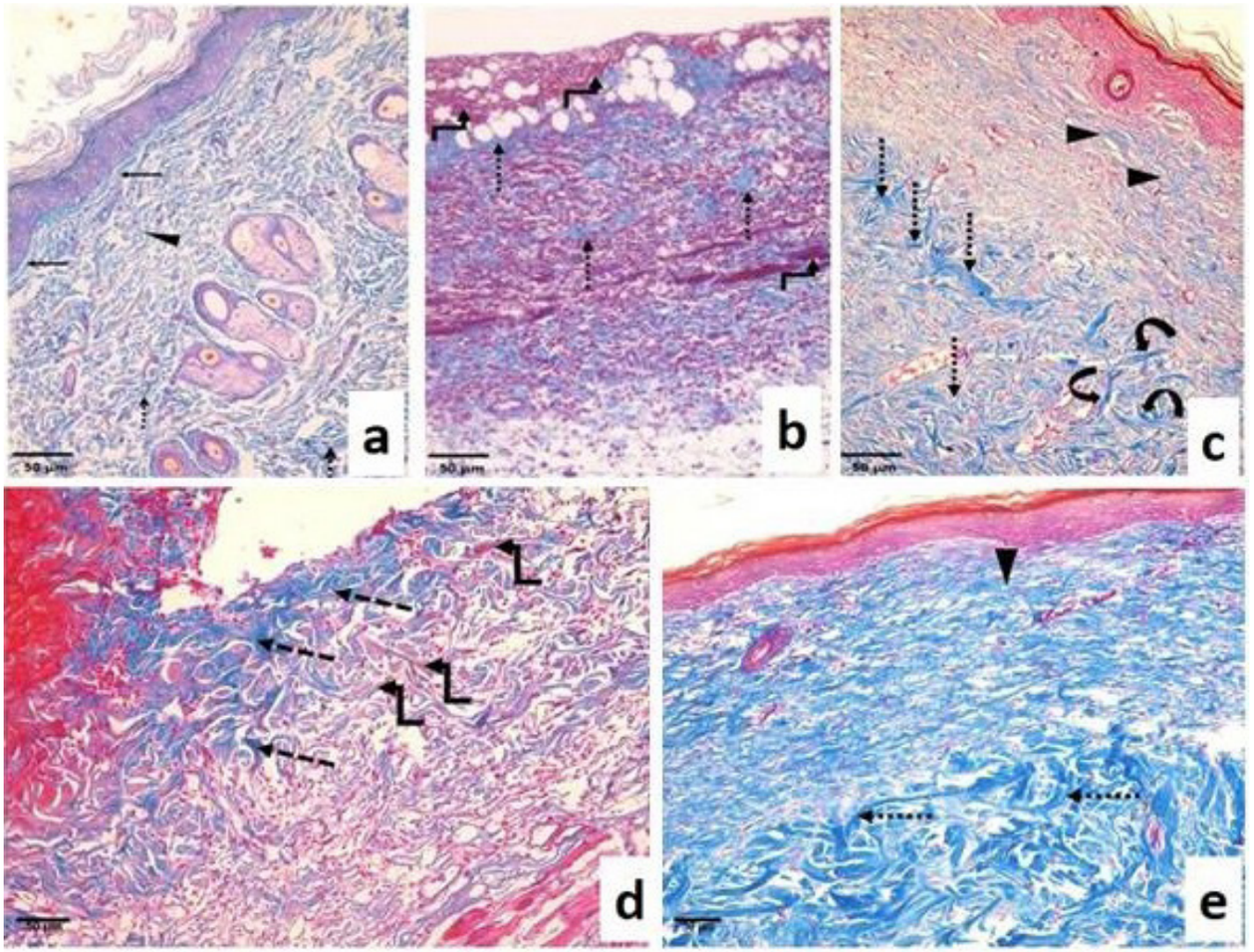

Fig. 13: Mallory's trichrome stained skin sections: (a) Control group: showing normal distribution of the dermal collagen fibers; beneath the basal lamina (arrow), in the papillary dermis as fine interlacing loosely arranged fibers (arrowhead) and in the reticular dermis as thick wavy bundles (dashed arrow) running in different directions. (b) Subgroup II-A: showing blue-stained thick wavy collagen bundles (dashed arrow) at the burn site. Some fused red-stained fibers (elbow arrow) are also noticed. (c) Subgroup II-B: showing fine horizontally arranged collagen fibers (arrowhead) in the superficial dermis and thicker collagen bundles in the deep dermis with some of them are running parallel to each other (dashed arrow) while others are running in different directions (curved arrow). (d) Subgroup III-A: showing thick, blue-stained irregularly arranged collagen fibers (dashed arrow) and red-stained fibers (elbow arrow) at the burn site. (e) Subgroup III-B: showing well-organized parallel blue-stained collagen fibers (arrowhead) in the superficial dermis and thick densely packed blue-stained collagen bundles (dashed arrow) running in different directions in the reticular dermis. (Mallory's trichrome, X 200, scale bar = 50μm)

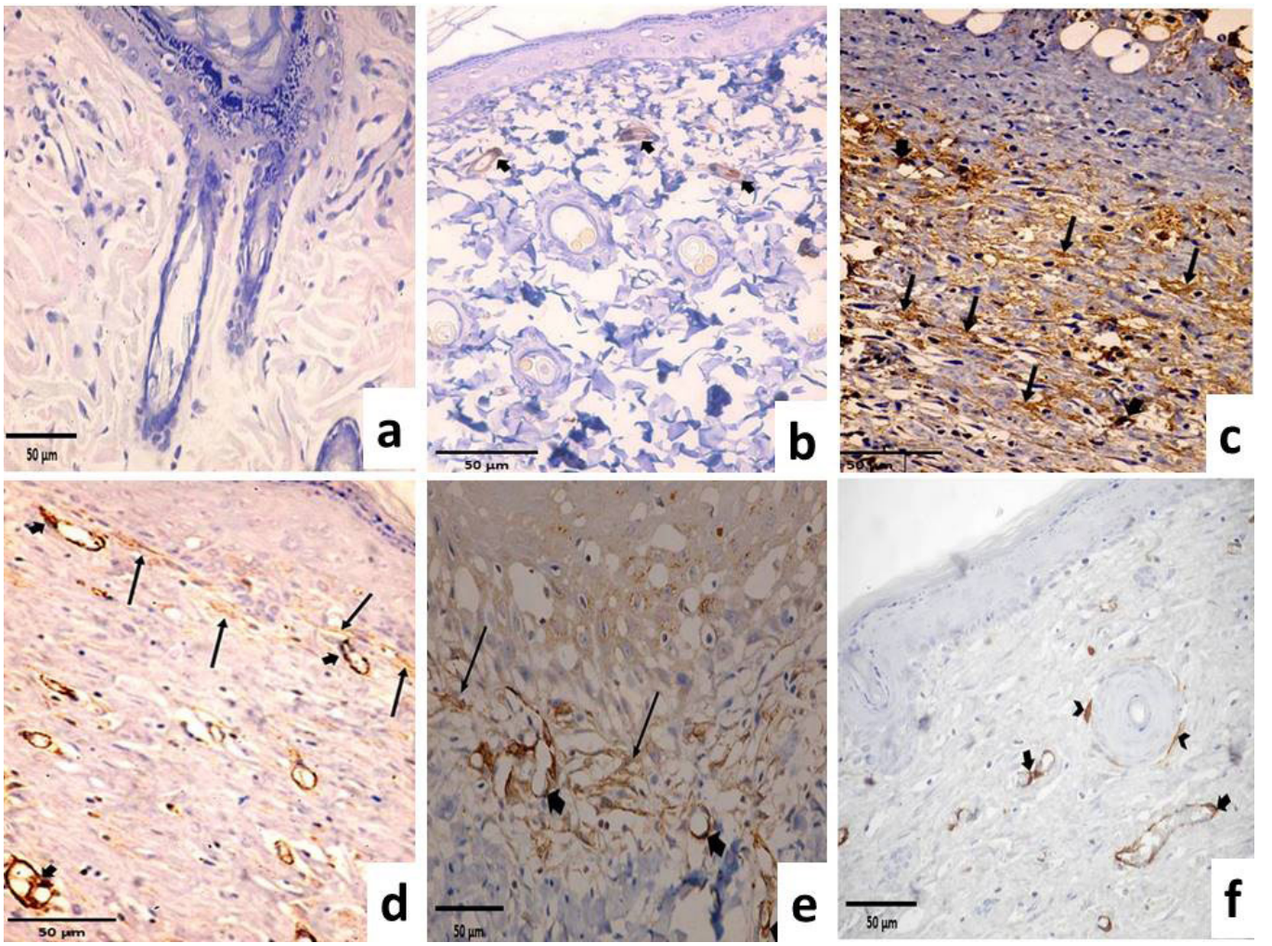

Fig. 14: Anti α-SMA stained skin sections: (a) Negative Control section: showing no immunoreaction. (b) Positive control section: showing cytoplasmic brownish reaction in the pericytes (thick arrow). (c) Subgroup II-A: showing apparent intense positive cytoplasmic brownish reaction in dermal myofibroblasts (thin arrow) and in pericytes (thick arrow). (d) Subgroup II-B: showing apparent moderate positive cytoplasmic brownish reaction in the dermal myofibroblasts (thin arrow) and an intense positive reaction in the pericytes (thick arrow) of the newly formed blood capillaries of the healing dermis. (e) Subgroup III-A: showing apparent intense positive brownish reaction in the cytoplasm of the dermal myofibroblasts (thin arrow) and pericytes (thick arrow). (f) Subgroup III-B: showing apparent intense positive brownish reaction in the pericytes cytoplasm (thick arrow) of the newly formed blood capillaries within the dermis and in the perifollicular sheath (arrowhead). (α-SMA immunostaining & Hematoxylin counter stain, X 400, scale bar = 50µm)

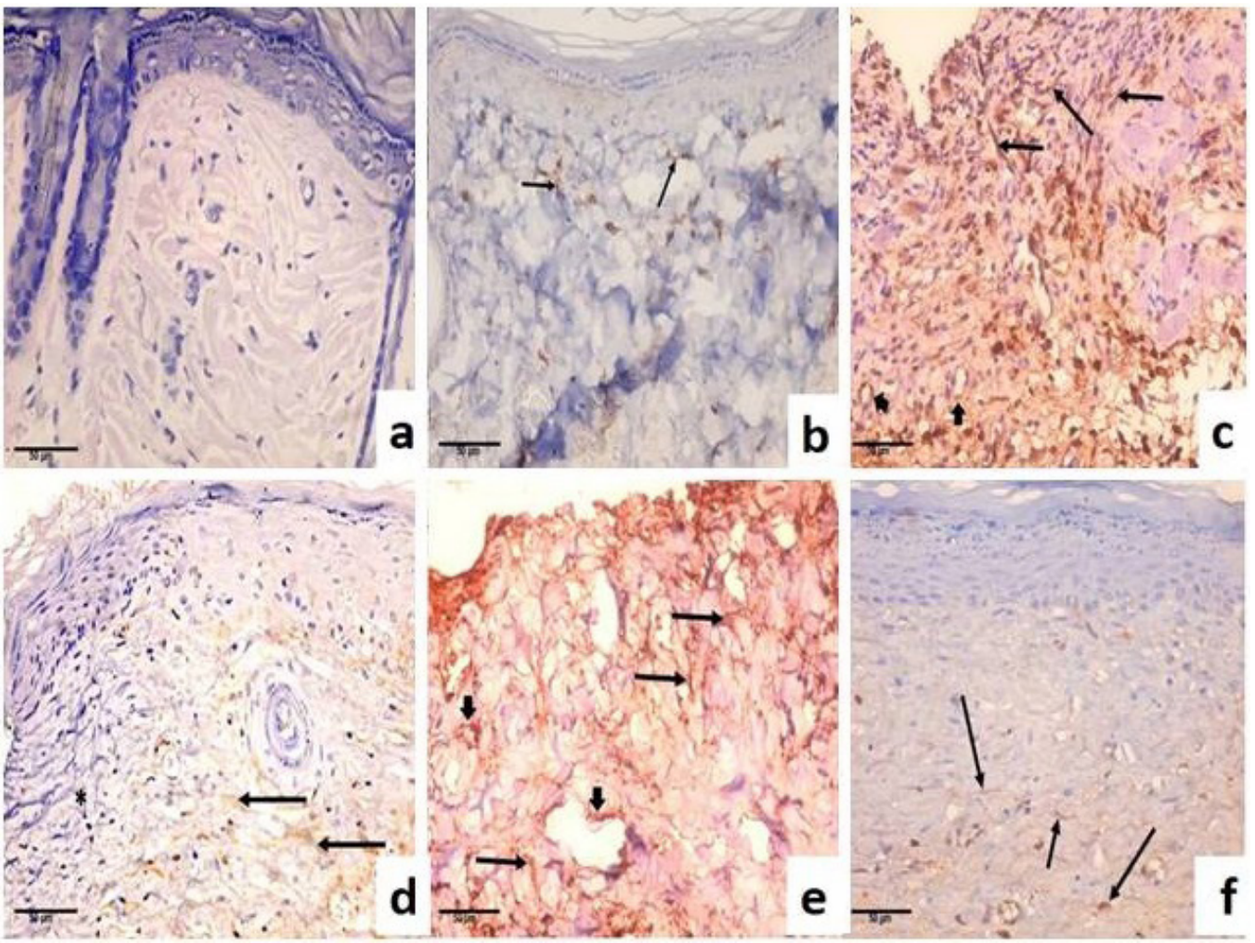

Fig. 15: Anti CD34 stained skin sections: (a) Negative Control section: showing no immunoreaction. (b) Positive control section: showing membranous expression of CD34 in some dermal spindle-shaped (dendritic) cells (thin arrow). (c) Subgroup II-A: showing intense cytoplasmic brownish reaction in many dermal spindle-shaped dendritic cells (thin arrow) and apparent moderate positive reaction in the blood capillaries endothelial cells (thick arrow). (d) Subgroup II-B: revealing moderate positive brownish reaction in the membrane of dermal spindle-shaped dendritic cells (thin arrow) surrounding the healing area. No dendritic cells were observed within the healed tissue (asterisk). (e) Subgroup III-A: showing strong positive brownish reaction in the cell membranes of dermal spindle-shaped dendritic cells (thin arrow) and in the endothelial cell cytoplasm of the blood capillary (thick arrow). (f) Subgroup III-B: showing moderate positive membranous brownish reaction in the spindle-shaped (dendritic) cells (thin arrow) present in the healing dermis. (CD34 immunostaining & Hematoxylin counter stain, X 400, scale bar = 50µm

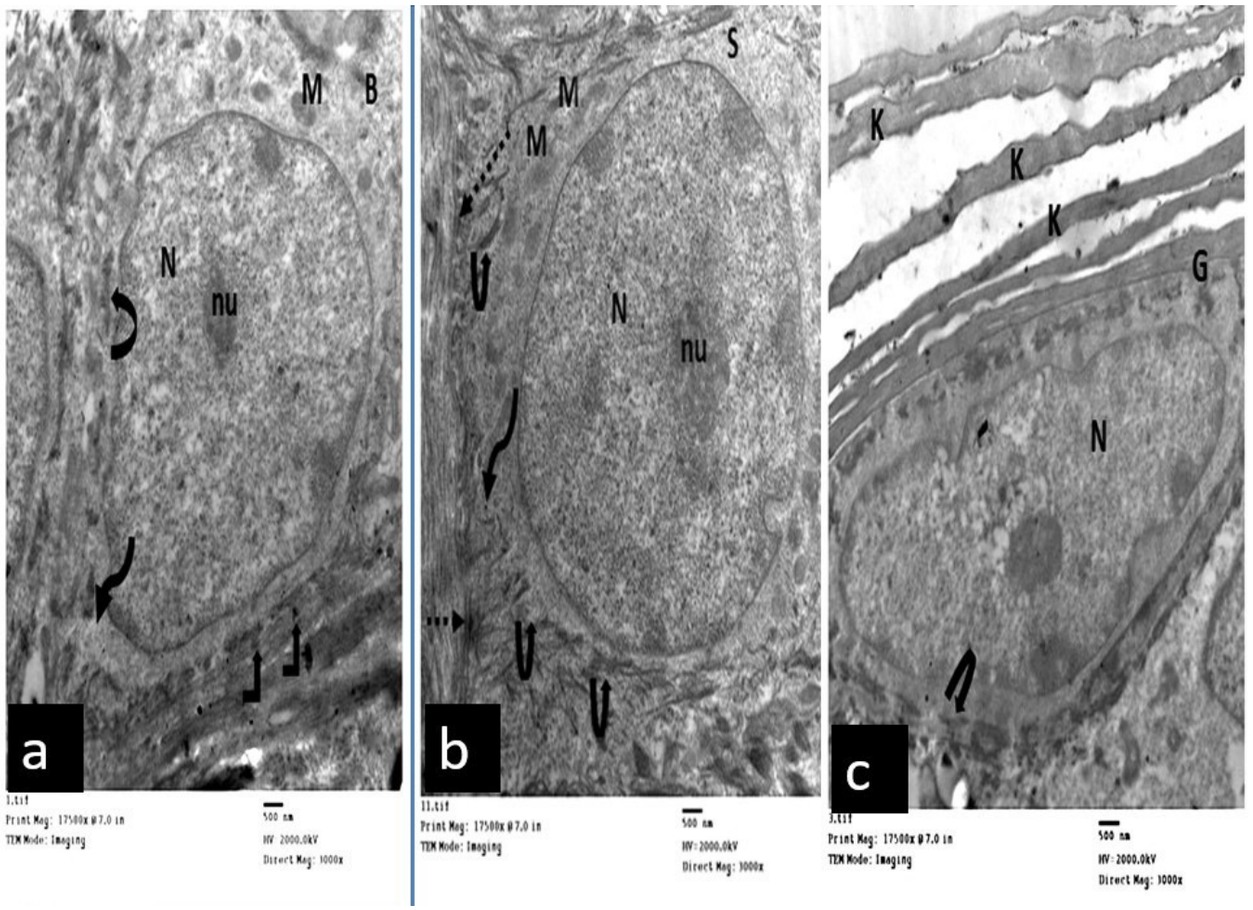

Fig. 16: Transmission electron micrographs of the control group showing: (a) A low columnar cell of stratum basale (B) with oval pale nucleus (N) and prominent nucleolus (nu). The cytoplasm shows free ribosomes (wavy arrow), mitochondria (M) and few tonofilaments (curved arrow). Notice the thin continuous basement membrane with multiple hemidesmosomes (right-angled arrow). (b) A stratum spinosum polyhedral cell (S) with oval to round euchromatic nucleus (N) containing prominent nucleolus (nu). The cytoplasm reveals free ribosomes (wavy arrow), mitochondria (M) and excess tonofibrils (curved arrow). Multiple desmosomes (dashed arrow) are noticed. (c) A stratum granulosum cell with flattened nucleus (N), multiple cytoplasmic variable sized electron dense keratohyalin granules (G) and aggregates of tonofibrils (curved arrow). Regularly arranged parallel homogenous keratin lamellae (K) of the stratum corneum are present. (a,b,c X 3000, scale bar = 500 nm)

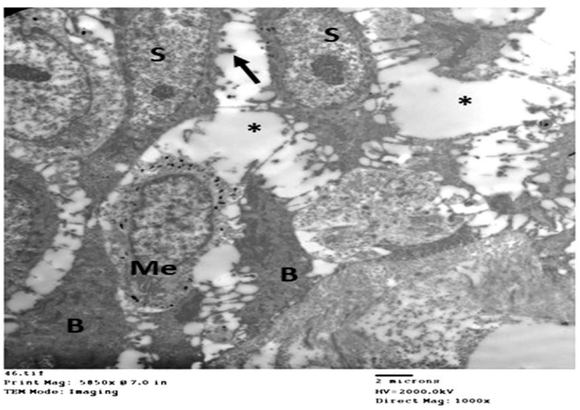

Fig. 17: Transmission electron micrograph of subgroup II-A showing a part of the epidermal tongue. Cells of stratum basale (B) are shrunken with dense cytoplasm. Interrupted desmosomal intercellular junctions (arrow) and wide intercellular spaces (asterisk) are noticed inbetween cells of stratum spinosum (S). A melanocyte (Me) containing multiple melanosomes is observed among the stratum basale. (X 1000, scale bar = 2 nm)

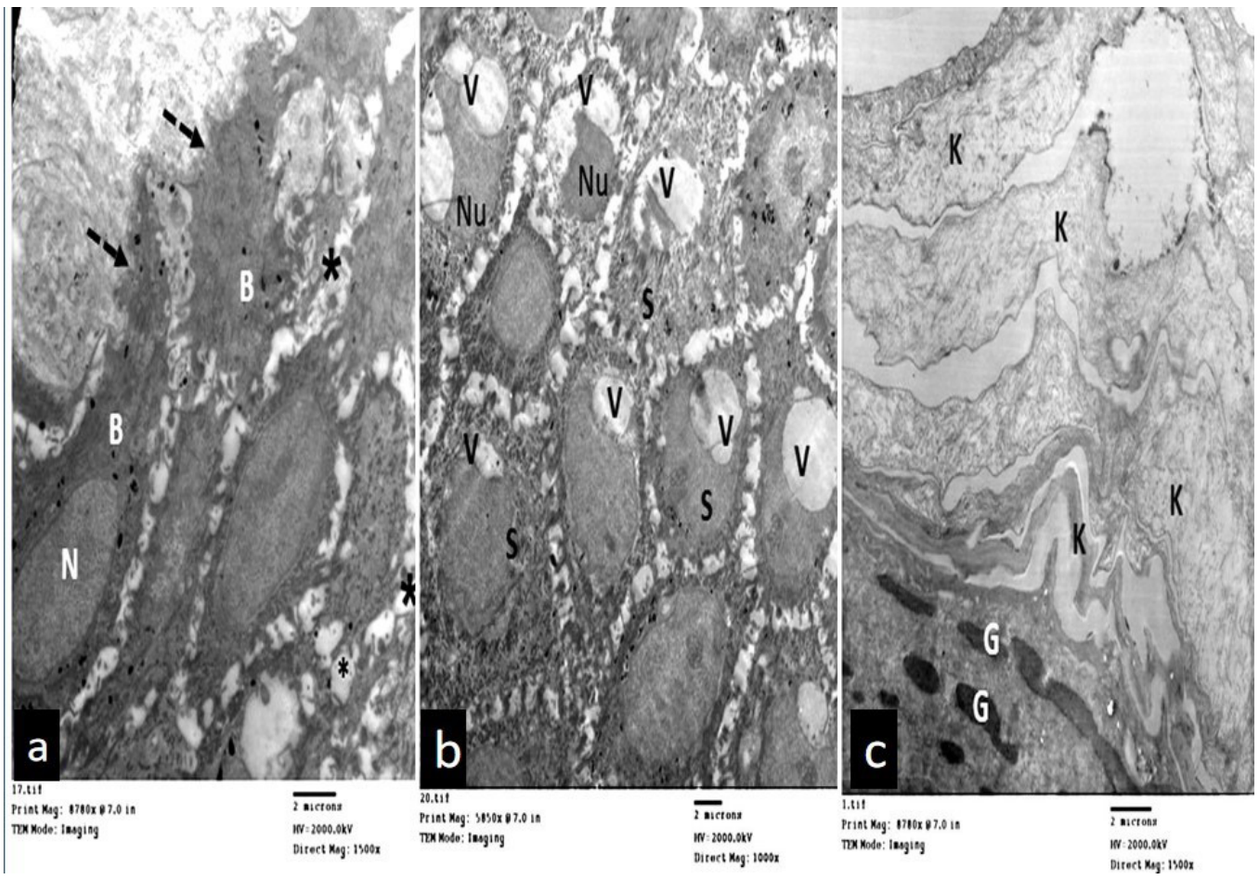

Fig. 18: Transmission electron micrographs of subgroup II-B showing: (a) Stratum basale cells (B) with flattened nuclei (N) and wide intercellular spaces (asterisk) between the keratinocytes with ill-defined basement membrane (dashed arrow). (b) Cells of stratum spinosum (S) with cytoplasmic vacuolation (V) and some shrunken nuclei (Nu). (c) Irregular disorganized thick and loosely packed keratin lamellae (K) of the stratum corneum. Keratohyalin granules (G) of stratum granulosum are noticed. (a, c X 1500, b X 1000, scale bar = 2 µm)

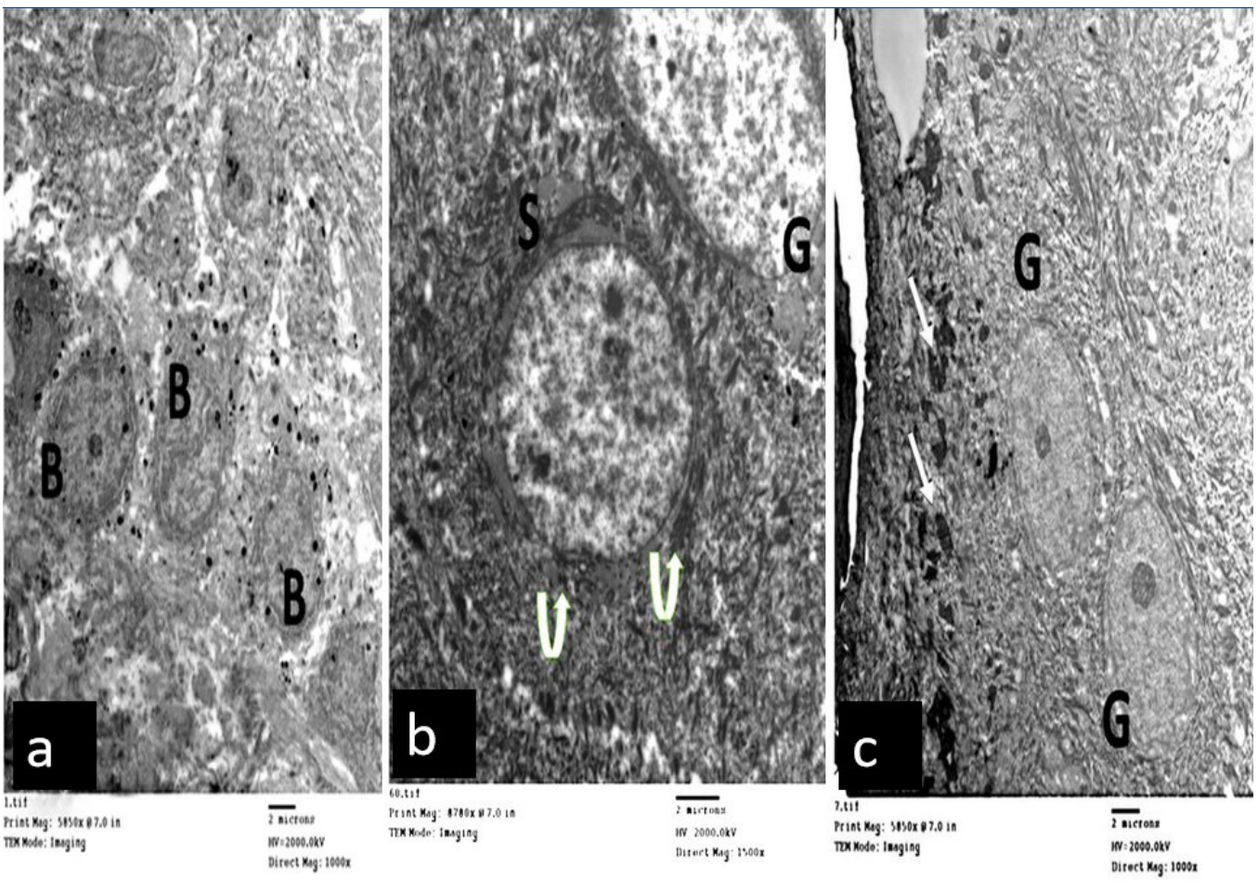

Fig. 19: Transmission electron micrographs of a part of an epidermal tongue of subgroup III-A showing: (a) Stratum basale cells (B) with many melanosomes. (b) A stratum spinosum cell (S) containing many cytoplasmic tonofilaments (curved arrow. A part of stratum granulosum cell with a flattened nucleus is also noticed. (c) Flattened stratum granulosum cells (G) with their characteristic keratohyalin granules (arrow). (a, c X 1000, b X 1500, scale bar = 2 μm)

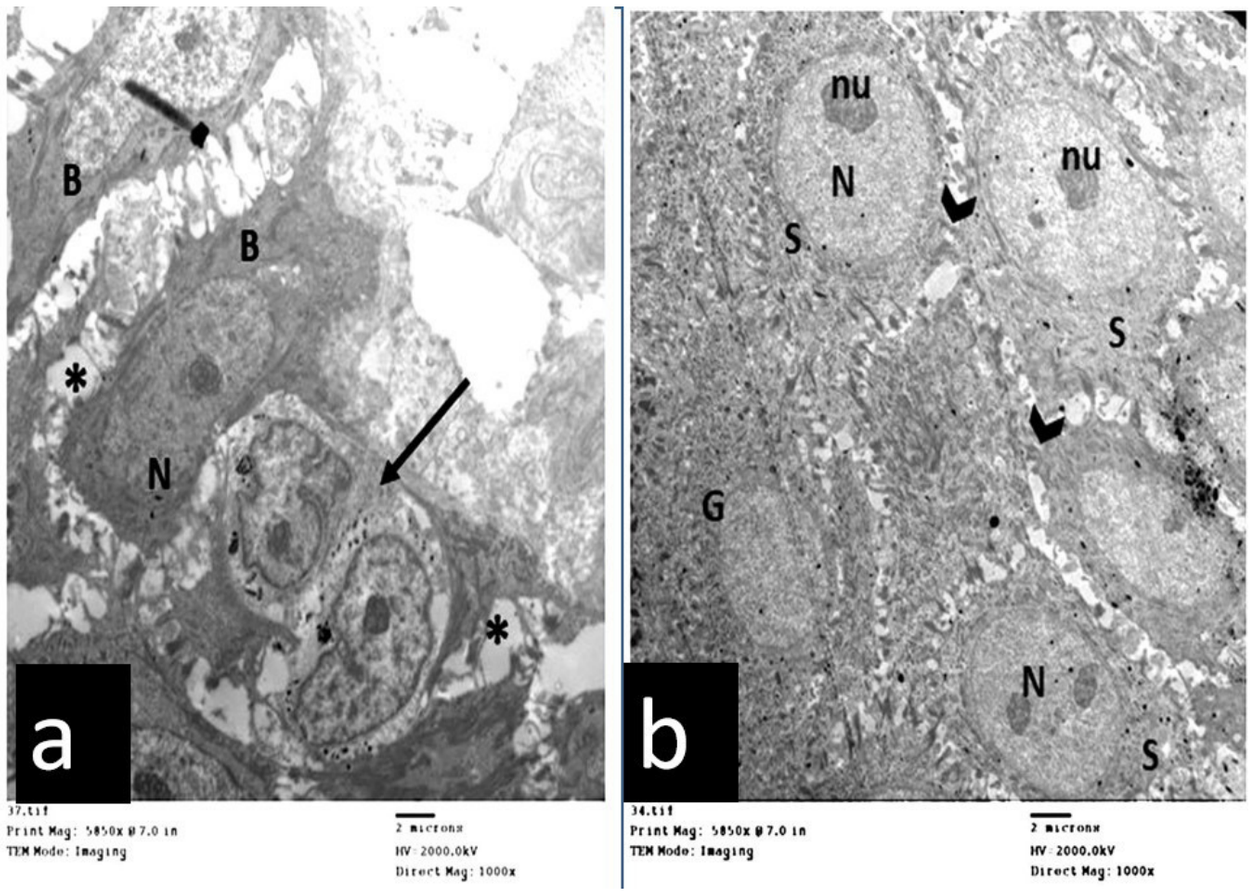

Fig. 20: Transmission electron micrographs of subgroup III-B showing: (a) columnar stratum basale cells (B) with oval basal nuclei (N) and wide intercellular spaces (asterisk) in between. A Langerhans cell (arrow) with an irregular indented nucleus and many lysosomes is also observed. (b) Polyhedral stratum spinosum cells (S) with central rounded nuclei (N), prominent nucleoli (nu) and multiple desmosomal junctions (arrowhead) in between. Stratum granulosum cells (G) are observed with their characteristic keratohyalin granules (dashed arrow). (a,b X 1000, scale bar = 2 µm)

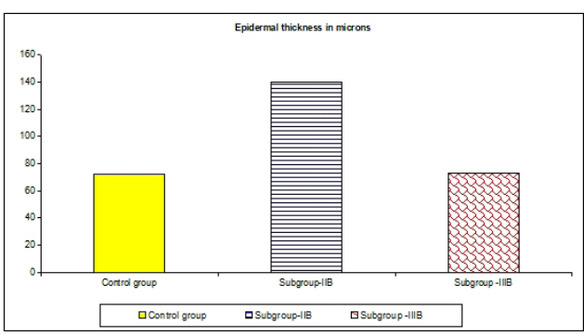

Fig. 21: Mean epidermal thickness in µm.

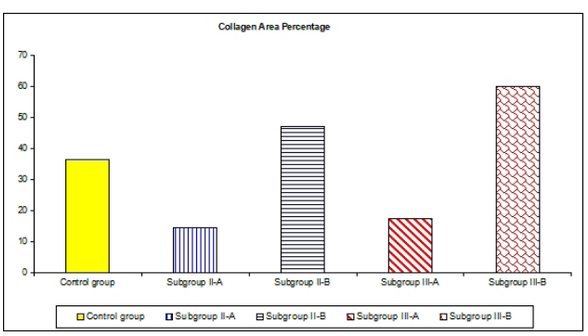

Fig. 22: Mean area percentage of collagen fibers.

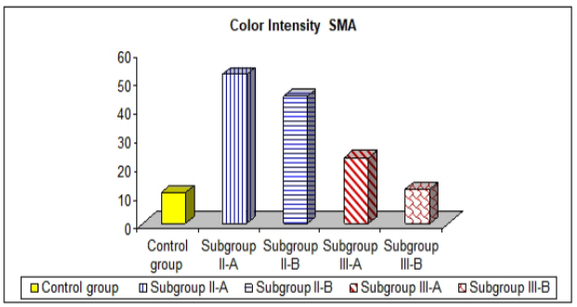

Fig. 23: Color intensity of α SMA immunoreaction.

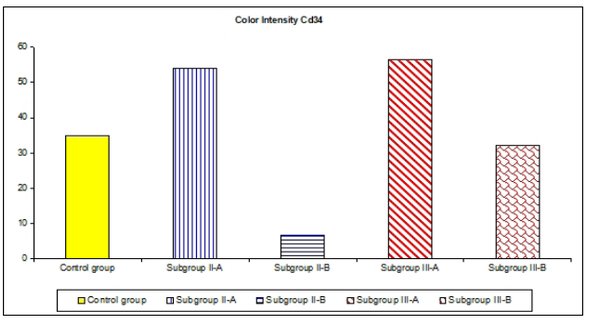

Fig. 24: Color intensity of CD34 immunoreaction.

Table 1: Mean epidermal thickness in µm.

Epidermal thickness	Control group	Subgroup II-B	Subgroup III-B
Mean ± SD	72.4 ± 9.5	139.8 ± 24.9	72.9 ± 24.9
F test		161.866	
P value		Less than 0.001**	
		T. Test	
Control & II-B	Control & III-B		II-B & III-B
< 0.001**	>0.05		< 0.001**

* means significant difference ** means highly significant difference

Table 2: Mean area percentage of collagen fibers.

Collagen Area Percentage	Control group	Subgroup II-A	Subgroup II-B	Subgroup III-A	Subgroup III-B
Mean ± SD	36.3 ± 8.7	14.6 ± 2.5	46.9 ± 8.2	17.3 ± 9.9	59.7 ± 15.7
F test		46.03			
P value		< 0.001**			

T. Test

Control & II-A	Control & II-B	Control & III-A	Control & III-B	II-A& II-B	II-A& III-A	II-B& III-B	III-A& III-B
< 0.001**	< 0.05*	< 0.001**	< 0.001**	< 0.001**	> 0.05	< 0.001**	< 0.001**

* means significant difference ** means highly significant difference

Table 3: Color intensity of anti α smooth muscle actin immunoreaction

Color Intensity of α-SMA	Control group	Subgroup II-A	Subgroup II-B	Subgroup III-A	Subgroup III-B
Mean ± SD	10.8 ± 3.3	52.1 ± 8.9	44.4 ±10.3	23 ± 8.2	12 ± 6.8
F test			80.3		
P value			< 0.001**		

T. Test

Control & II-A	Control & II-B	Control & III-A	Control & III-B	II-A& II-B	II-A& III-A	II-B& III-B	III-A& III-B
< 0.001**	< 0.001**	< 0.001**	> 0.05	< 0.05*	< 0.001**	< 0.001**	< 0.001**

* means significant difference ** means highly significant difference

Table 4: Color intensity of CD34 immunoreaction

Color Intensity of Cd34	Control group	Subgroup II-A	Subgroup II-B	Subgroup III-A	Subgroup III-B
Mean ± SD	34.995 ±	54.112.7 ±	6.64.2±	56.8.4 6±	32.2 ± 14.2
F test			56.2		
P value			< 0.001**		

T. Test

Control & II-A	Control & II-B	Control & III-A	Control & III-B	II-A& II-B	II-A& III-A	II-B& III-B	III-A& III-B
< 0.001**	<0.001**	< 0.001**	>0.05	< 0.001**	>0.05	< 0.001**	< 0.001**

* means significant difference ** means highly significant difference

DISCUSSION

Burn is considered one of the most destructive skin injuries that causes more than one million deaths each year in addition to million cases of disability. Patients with large burn wounds usually suffer from slow healing and are more susceptible to infection and subsequent hypertrophic scars. The later occurs because of excessive thick, hyalinized collagen production together with excessive formation of extracellular matrix by the proliferating fibroblasts[25].

Yet, researchers and clinicians have a great challenge in developing new proper early treatment of burn wounds in order to prevent or improve hypertrophic burn scars and their devastating consequences.

Platelet-rich plasma is a method proposed for wound treatment. It was proved to enhance healing after soft tissue and orthopedic injuries through secretion of cytokines, chemokines and interleukins in addition to multiple growth factors[26]. These factors involve epidermal growth factor (EGF) in addition to many other growth factors. Moreover, fibrinogen, osteocalcin, osteonectin and fibronectin are also secreted from platelets when activated[27].

The present work aimed to assess the potential therapeutic influence of PRP on the healing of second-degree skin burn and the possible prevention of scar formation in adult male albino rat by means of diverse histological techniques.

In the current study, subgroup II-A (the burnt rats examined after one week of burn induction) showed an area of epidermal discontinuity at the burn site that was occupied in some sections by a scab with presence of underlying granulation tissue. A migratory epidermal tongue was also observed at the edge of the wound. These findings agreed with the results of Pereira *et al*., (2012)[9]. In addition, Xian *et al*., (2015)[28] observed the epithelial cells migration beneath the scab formed after two days of healing of full-thickness skin incision wounds. These findings could be explained according to Heng, (2011)[29] who illustrated that the skin barrier is disrupted after acute skin injury with attraction of neutrophils, monocytes in addition to macrophages to the injury site with subsequent keratinocytes activation. Some of the activated keratinocytes migrate into the wound to fill the defect, whereas the other keratinocytes proliferate.

Flattened migratory stem cells were noticed at the burn edge of the superficial dermis in subgroup II-A. This agreed to the results of Eldrieny *et al*., (2014)[30] and could be explained according to Chen *et al*., (2015)[31] who stated that the dermal stem cells are stimulated by the macrophages present in the inflammatory infiltrate upon skin injury, resulting in hair follicle and sebaceous gland stem cell proliferation and migration toward the injured tissue.

Intense inflammatory mononuclear cellular infiltrate and dilated blood capillaries as well as fibroblasts proliferation that were observed in subgroup II-A, were also reported by Ozcelik *et al*., (2016)[32] in untreated burn wounds. These observations could be explained according to Baum & Arpey, (2005)[33] who demonstrated that the inflammatory stage at the skin wound is prompted by exudate clotting and platelet degranulation which involves histamine, serotonin and bioactive factors release, causing a surge in the capillary permeability with subsequent inflammatory cells migration .

Boothby *et al*., (2020)[34] added that neutrophils reach their maximum infiltration at the injury site within the first two days after injury. Together with macrophages, neutrophils play a principal role in activating keratinocytes, fibroblasts and immune cells as well as minimizing incidence of bacterial infection of the wounds. When the stage of inflammation is about to end, the macrophages change to their anti-inflammatory profibrotic phenotype secreting interleukins, TGF-β and tumor necrosis factor (TNF). The former growth factors enhance the onset of the proliferative stage[35]. However, excessive inflammation, especially with the presence of a high number of macrophages upon burn injury, was found to form a hypertrophic scar[36].

Hypertrophic scar involves the presence of fibrous tissue with parallel horizontally oriented collagen bundles instead of the normal papillary and reticular dermis, in addition to increased blood vessels density and hyperproliferative keratinocytes[37,38]. After the re-epithelization is complete, it takes 24 weeks for the scar tissue to become mature[39]. Early immature scar shows more inflammatory cells, more blood vessels and fine parallel collagen bundles. As the scar matures, the inflammatory cells decrease, the density of the blood vessels decreases while the collagen fibers become organized into thicker dense bundles[40,41].

In the current study, subgroup II-B showed appearance of thick keratinized epidermis with a highly significant increase in its mean thickness as compared to the control group. Focal aggregations of keratin lamellae were also observed. These observations agreed with the observations of Wen *et al*., (2015)[41] and could be explained according to Galko & Krasnow, (2004)[42] who earlier demonstrated that upon thermal injury, the wound margin become exposed to high levels of mechanical stress which sequentially stimulate hypertrophic scar formation through enhancing cellular proliferation and keratin accumulation.

The basement membrane underlying the stratum basale was focally ill-defined in the epidermis of subgroup II-B. This agreed with Ramos-Lewis *et al*., (2018)[43] who also reported that it took a long time to restore the normal appearance of the basement membrane after skin injury. Yang *et al*., (2016)[38] explained this finding by diminished collagen IV deposition beneath the epidermis together with suppressed expression of integrin β4 in the basale layer of the epidermis. They also stated that altered formation of the basement membrane results in increased proliferation of the keratinocytes of the scarred epidermis and thus affecting re-epithelialization and tissue remodeling, which in turn results in hypertrophic scar formation.

Vacuolated cytoplasm was observed in cells of stratum basale, spinosum and granulosum in subgroup II-B. Kim *et al*., (2011)[44] attributed the cytoplasmic vacuolation to be the result of excess reactive oxygen species (ROS) resulting from thermal injury.

Wide intercellular spaces were also observed in the same subgroup. Similar finding was reported and explained by Younan *et al*., (2010)[45] and Tanaka *et al*., (2013) [46] to be the result of perivascular edema secondary to increased permeability and water leak from the capillaries following thermal injury. Previously, Mahoney *et al*., (2010)[47] attributed wide intercellular spaces to be the result of weakening of cellular adhesion secondary to down regulation of the adhesive molecules of the desmosomes and other junctional complexes. Extravasation was also observed in the untreated subgroup IIB. This could be appertaining to the prolonged inflammatory phase with the subsequent platelet degranulation releasing histamine, heparin and other cytokines, causing increased capillary permeability[27].

Instead, treatment of the burnt skin with PRP in group III gave better results than untreated group II that were more prominent in subgroup III-B than subgroup III-A. H&E-stained skin sections obtained from subgroup III-B revealed nearly complete epidermal regeneration with more or less normal epidermal layers that showed a non-significant difference in its mean thickness as compared to the control group. In addition, angiogenesis and grouped hair follicles were noticed in the dermis.

Carter *et al*., (2003)[27] stated that the inflammatory phase is reduced in wounds treated with PRP through minimizing the incidence of bacterial infections and scars formation. Recently, Everts *et al*., (2020)[48] demonstrated that platelets secrete pro-inflammatory cytokines that may induce a mild pro-inflammatory reaction provoking the wound healing. However, PRP also secretes anti-inflammatory cytokines that shorten the duration of the inflammatory process.

Kim *et al*., (2011)[44] reported that PRP exhibited a bio-regenerative action through enhancing fibroblastic proliferation as well as secreting anti-inflammatory factors, angiogenic factors and the proteins concerned with the remodeling of extracellular matrix. Therefore, PRP is generally used clinically in treatment of chronic lesions, as diabetic ulcers[49]. In addition, Behm *et al*., (2012)[50] confirmed the role of PRP in controlling oxidative damage and hence decreasing inflammation and scar formation.

The process of angiogenesis observed in subgroup II-B means new blood vessels formation. This ensures sufficient oxygen and nutrients supply and helps to discard metabolic waste products. This process is essential for cell proliferation[51]. In subgroup III-B, the angiogenetic vessels appeared enlarged, thin-walled and septated. This agreed with the findings of Pettersson *et al*., (2000)[52] who mentioned that angiogenesis is a vital process in wound healing that is essential for keratinocytes survival and for preserving the newly formed granulation tissue. The influence of PRP on angiogenesis could be clarified according to Zhang *et al*., (2019)[53] who stated that the VEGF present in platelets α granules stimulates the endothelial cells resulting in their activation, proliferation and migration resulting in new capillary formation.

Tonnesen *et al*., (2000)[54] and Hammam *et al*., (2019)[55] also demonstrated that the endothelial cells invade the underlying vascular basement membrane and extracellular matrix (ECM), then branch to form new vessels. Xu *et al*., (2020)[56] added that PRP enormously improves skin wound healing by stimulation of angiogenesis and re-epithelialization in addition to local inflammation control by inhibition of interleukin-17A and interleukin-1β secretion.

Multiple grouped hair follicles were observed in treated subgroup III-B. Rognoni *et al*., (2016)[57] revealed that hair follicles regenerate after healing of skin wounds and usually appear in small clusters surrounded by scar tissue. Gentile & Garcovich, (2020)[58] added that PRP could promote the cycle of hair growth and help the reconstruction of hair follicle, therefore, it has been recently used clinically in treatment of cases of alopecia.

As regards Mallory's trichrome-stained sections, subgroup II-A revealed thick blue-stained collagen bundles at the burn site together with appearance of some red fused collagen fibers. This agreed with Nicoletti *et al*., (2019)[59] who observed thick collagen fibers at day 10 after burn and also with Chen *et al*., (2016)[60] and Nassar *et al*., (2017)[61] who observed red-stained fused collagen fibers, one week after burn. The later authors explained these changes to be due to loss of crystallinity of collagen fibers. In addition, this subgroup revealed a highly significant diminution in the mean area percentage of collagen fibers when compared with the control group.

Meanwhile, subgroup II-B revealed well-organized collagen fibers arranged parallel to the epidermis in the papillary dermis and thick collagen fibers in the reticular dermis, some running parallel while others running in different directions. Statistical analysis of the mean area percentage of collagen fibers of this subgroup revealed a highly significant increment in respect to the control group. Kim *et al*., (2019)[62] reported that during the regeneration process, the fibroblasts synthesize collagen type III, that is substituted by type I collagen afterward. They also added that the scar tissue collagen has a unidirectional arrangement. Furthermore, Li **et al**., (2007)[63] stated that a period of two months is needed for the collagen fibers at the injury site to return to the completely normal arrangement as that of the intact tissue.

On the other hand, subgroup III-A revealed presence of thick collagen bundles in addition to some red-stained collagen fibers. This result was non-statistically different from the corresponding untreated subgroup II-A. However, subgroup III-B showed almost normal organization of collagen fibers in the form of well-organized fibers in the

superficial dermis and thick fibers running in different directions in the reticular dermis. Moreover, subgroup III-B showed a highly significant increase in mean area percentage of the collagen fibers in respect to both control group and subgroup II-B.

These results came in line with Yildiz *et al*., (2016)[64] who reported a statistical surge in collagen fibers deposition in the groups treated by PRP. Moreover, Gurtner *et al*., (2008)[35] referred to that both density and organization of the collagen fibers affect the scar formation.

In the present work, the better statement and arrangement of collagen fibers in the PRP-treated subgroup III-B than the untreated subgroup II-B indicated that one PRP injection enhances remodeling. However, Nofal *et al*., (2014)[65] attempted triple PRP injections for better results, so that repeated PRP injections may increase collagen synthesis.

The PRP role in the remodeling of collagen is still unclear, as stated by Ibrahim *et al*., (2015)[66], who mentioned that it depends on matrix metalloproteinases (MMP), particularly MMP-1 and MMP-3. They added that MMP-1 induction in the skin could enhance the elimination of the dermal damaged fragments of collagen and consequently provides enhances new collagen deposition. Additionally, Kim *et al*., (2011)[44], in their research on ECM remodeling, noticed that PRP enhanced collagen type I and MMP-1 matrix metalloproteinase synthesis and also increased mRNA expression in the fibroblasts of the human dermis. This resulted in ordered arrangement and uniform density of collagen, and as the scar matures, the collagen bundles became thicker and arranged in different directions instead of being parallel to the surface.

Myofibroblasts represent the principle cell in wound closure[67]. In the present work, we assessed the myofibroblasts role by evaluating the immunohistochemical expression of α-SMA and statistically analyzing its color intensity in the immunostained sections.

The untreated subgroups II-A and II-B revealed a strong positive expression of α SMA in the dermal myofibroblasts and pericytes with a highly significant increment in its color intensity in respect to the control group. Instead, subgroup II-B showed a significant decrement in α-SMA color intensity compared to subgroup II-A.

Sorg *et al*., (2017)[67] stated that four days after injury, the fibroblasts differentiate into myofibroblasts then express α-SMA. This differentiation is promoted by PDGF and TGF-β1 secreted by the inflammatory cells in the injured tissue. Moreover, Kwan *et al*., (2009)[68] stated that a contractile force is exerted by the myofibroblasts through actin myofilaments that are linked focally to the ECM. This allows the wound edges to approximate at a rate of 0.75 mm per day, which helps wound healing. However, after closure of the wound, the myofibroblasts undergo apoptosis as the epithelialization process is already complete. If the myofibroblasts persist after wound closure, the wound contraction will continue resulting in excessive fibrosis with poor cosmetic results ending in developing hypertrophic scar[69].

Regarding PRP-treated group, subgroup III-A revealed an intense positive reaction in both dermal myofibroblasts and pericytes. Meanwhile, subgroup III-B showed an intense positive reaction in pericytes of the newly formed blood capillaries and in the perifollicular sheath. Statistically, subgroup III-A showed a highly significant increment in the color intensity of anti α SMA as compared to the control group while subgroup-IIIB revealed a non-significant difference from the control group. Moreover, both subgroups III-A and III-B exhibited a highly significant diminution in anti α-SMA color intensity in respect to the corresponding untreated subgroups II-A and II-B respectively. Moreover, subgroup III-B revealed a highly significant diminution in anti α SMA color intensity as compared to subgroup III-A. This agreed with the findings of Chellini *et al*., (2018)[70] who proved that PRP enormously diminished the effect of TGF-β on differentiation of the myofibroblasts through reduction of assembly of stress fiber and down regulation of α-SMA.

Skin has epidermal Langerhans cells and dermal dendritic cells. Both cells are considered antigen presenting cells[71]. Limandja *et al*., (2020)[72] demonstrated that dermal dendritic cells are absent in hypertrophic immature scars and present in mature scars. Therefore, the present study evaluated the immunohistochemical expression of CD34 (a marker for the dermal dendritic cells) and statistically analyzed the color intensity of its expression.

In the present work, subgroup II-A revealed an intense positive reaction for CD34 in cytoplasm of endothelial cells and pericytes of the dermal blood capillaries in addition to the cell membranes of multiple dermal spindle-shaped (dendritic) cells. Those dendritic cells were not detected in the scar tissue in subgroup II-B, although being abundant in the peri-cicatricial tissue (the area around the healing dermis). Statistical analysis of color intensity of CD34 expression revealed a highly significant increment in subgroup II-A as compared to the control group and a highly significant diminution in subgroup II-B as compared to both the control group and subgroup II-A. These results agreed with those of Erdag *et al*., (2008)[71], who reported absence of CD34 positive dendritic cells in scars and their increase in the tissue surrounding scars.

The previous authors added that the absence of CD34 positive cells within the scar tissues and their increase in the surrounding tissues may reveal a role of CD34 positive cells in collagen synthesis regulation, wound healing and scar formation. Furthermore, Limandja *et al*., 2020[72] reported decreased expression of CD34 with decreased number or even absence of dermal dendritic cells in immature hypertrophic scars.

As regards the immunohistochemical expression of CD34 in PRP-treated subgroups, subgroup III-A showed an intense positive reaction in dermal dendritic cells,

endothelial cells and pericytes. Statistically, this subgroup revealed a highly significant increment in CD34 color intensity as compared to the control group while showing a non-significant difference from the corresponding untreated subgroup II-A. On the other hand, subgroup III-B expressed a moderately positive reaction in the dendritic cells together with a strong positive cytoplasmic reaction of the endothelial cells of the newly generating blood capillaries.

On the other hand, subgroup III-B, showed a highly significant decrement in CD34 color intensity in respect to both subgroups III-A and II-A while revealing a non-significant difference from the control group. These findings agreed to the observations of Limandja *et al*., (2020)[72] who stated that mature scars resemble normal skin in being CD34 positive due to presence of dermal dendritic cells. Accordingly, this suggests that PRP could enhance scar maturation.

As regards the electron microscopic study, results from both subgroups II-A and II-B confirmed the previous light microscopic results. Subgroup II-A showed presence of epidermal tongue. The cells appeared widely separated with focal separation of the basale cells from the underlying basement membrane. Some basale cells were shrunken with dense cytoplasm. Subgroup II-B showed ill-defined basement membrane with wide intercellular spaces in between the keratinocytes. Some spinosum cells showed cytoplasmic vacuolation and shrunken nuclei.

The shrunken nuclei and dense cytoplasm could be explained according to Raj *et al*., (2006)[73] to be signs of apoptotic cell death. The later represents a critical vital process that is essential for formation of the skin horney layer and in maintenance of normal epidermal structure through balancing proliferation of the keratinocytes.

Electron microscopic results obtained from the treated group supported the light microscopic results. Subgroup III-A showed epidermal tongue in addition to presence of mast cells in the dermis. However, subgroup III-B showed almost normal epidermal layers except for focal separation of some stratum basale cells.

CONCLUSION

According to the previously mentioned data, the current study illustrated that PRP exerted beneficial effect on healing of burn wound that was more prominent after four weeks from burn induction besides promoting the formation of mature scar instead of hypertrophic scar.

RECOMMENDATIONS

According to the results of this study, we recommend:

1. Early treatment of patients with thermal burn injuries with local PRP injection.
2. Further studies using multiple injections of PRP to assess their possible better effects than the single injection.
3. Further research to analyze the possible therapeutic effects of PRP on other types of burn injuries.
4. Clinical trials to estimate the potential beneficial effects of PRP on treatment of second-degree burn injuries in human.

CONFLICT OF INTERESTS

There are no conflicts of interest.

REFERENCES

1. Morgan ED, Bledsoe SC and Barker J. Ambulatory management of burns. American Family Physician 2000; 62(9):2015-2026.
2. Forbes-Duchart L, Cooper J, Nedelec B, Ross L and Quanbury A. Burn therapists' opinion on the application and essential characteristics of a burn scar outcome measure. Journal of burn care & research 2009; 30(5):792-800.
3. Peck M. Epidemiology of burns throughout the world. Part I: Distribution and risk factors. Burns 2011; 37(7):1087-1100.
4. Prochazka V, Klosova H, Stetinsky J, Gumulec J, Vitkova K, Salounova D, Dvorackova J, Bielnikova H, Klement P, Levakova V, Ocelka T, Pavliska L, Kovanic P. and Klement GL. Addition of platelet concentrate to dermo-epidermal skin graft in deep burn trauma reduces scarring and need for revision surgeries. Clinical Trials Gov. 2014; 158(2):242-258.
5. Finnerty C, Jeschke M, Branski L, Barret JP, Dziewulski P and Herndon DN. Hypertrophic scarring: the greatest unmet challenge after burn injury. Lancet 2016; 388(10052):1427-1436.
6. Aust M, Pototschnig H, Jamchi S and Busch KH. Platelet-rich plasma for skin rejuvenation and treatment of actinic elastosis in the lower eyelid area. Cureus 2018; 10(7):2999-3107.
7. Ching YH, Sutton TL, Pierpont YN, Robson MC and Payne WG. The use of growth factors and other humoral agents to accelerate and enhance burn wound healing. Eplasty 2011; 11(2):146-153.
8. Menetrey J, Kasemkijwattana C, Day CS, Bosch P, Vogt M, Fu FH, Fu MS and Huard J. Growth factors improve muscle healing in *vivo*. The Journal of bone and joint surgery. British volume 2000; 82(1):131-137.
9. Pereira T, Dos Santos D, Lima-Rebeiro, MHM, Pontes-Filho NT, Carneiro-Leão AMA and Correia MTS. Development of animal model for studying deep second-degree thermal burns. Journal of Biomedicine and Biotechnology 2012; 3(1):460841.
10. Huang SH, Wu SH, Lee SS, Lin YN, Chai C, Lai CS and Wang, HMD. Platelet-Rich Plasma Injection in Burn Scar Areas Alleviates Neuropathic Scar Pain. Int J Med Sci 2018; 15(3): 238-247.

11. Gaertner D, Hallman T, Hankenson F and Batcherder M. Anesthesia and analgesia for laboratory rodents, chapter 3, In Anesthesia and analgesia in laboratory animals. Academic Press, San Diego, CA. Boston. 2008; pp. 239.
12. Fish R, Danneman P, Brown M and Alicia K. Anesthesia and Analgesia in Laboratory Animals. Academic Press. 2011; pp. 65.
13. Cai EZ, Ang CH, Raju A, Tan KB, Hing ECH, Loo Y, Wong YC, Lee H, Lim J, Moochhala SM and Hauser CA. Creation of consistent burn wounds: a rat model. Archives of Plastic Surgery 2014; 41(4):317-325.
14. Parasuraman S, Raveendran R and Kesavan R. Blood sample collection in small laboratory animals. Journal of Pharmacology and Pharmacotherapeutics 2010; 1(2):87-95.
15. Beeton C, Garcia A and Chandy KG. Drawing blood from rats through the saphenous vein and by cardiac puncture. Journal of visualized experiments 2007; 12(7):266-276.
16. Dhurat R and Sukesh MS. Principles and methods of preparation of platelet-rich plasma: A review and author's perspective. Journal of Cutaneous and Aesthetic Surgery 2014; 7(4):189-197.
17. Turgeon ML. Clinical hematology - theory and procedures, 3rd edition. Lippincott Williams and Wilkins, Philadelphia. 1999; pp. 320.
18. Batra S. Total platelet count using hemocytometer / Neubaurs chamber (micro dilution and microdilution method): Paramedics world. 2018
19. Suavarna SK, Layton C and Bancroft JD. Plastic embedding for light microscopy in Bancroft's Theory and Practice of Histological Techniques. 7th edition, Churchill Livingstone, Elsevier, Philadelphia. 2013; pp.151.
20. Bikadi P, Szabo J, Szabara A and Jakab C. Internal positive controls of alpha-smooth muscle actin (a-SMA) in bovine tissues Immunohistochemical study. Magyar Allatorvosok Lapja 2015; 137(1):151-158.
21. Anggorowati N, Ratna Kurniasari CH, Damayanti K, Cahyanti T, Widodo I, Ghozali A, Romi MM, Sari DC and Arfian N. Histochemical and Immunohistochemical Study of α-SMA, Collagen, and PCNA in Epithelial Ovarian Neoplasm. Asian Pacific Journal of Cancer Prevention: APJCP 2017; 18(3):667-671.
22. Gulsun S, Qureshi W and Patterson R. CD34-positive dendritic cells disappear from scars but are increased in pericicatricial tissue. Journal of Cutaneous Pathology 2008; 35(8):752-756.
23. Jackson P and Blythe D. Immunohistochemical techniques, chapter 4, in: Theory and Practice of Histological Techniques. By: Bancroft JD and Gamble M (eds): 6th edition. Chuchill Livengstone. London, Sydney, New York, Toronto. 2008; pp: 433.
24. Kuo J. Processing Biological Tissues for ultrastructural study in Electron Microscopy: Methods and Protocols. 2nd edition, Humana Press Inc. Totowa, New Jersey 2007; pp .19.
25. Dong Y, Cui M, Qu J, Wang X, Kwon SH, Barrera J, Elvassore N and Gurtner GC. Conformable hyaluronic acid hydrogel delivers adipose-derived stem cells and promotes regeneration of burn injury. Acta Biomaterialia 2020; 108(1):56-66.
26. Hultman CS, Friedstat JS, Edkins RE, Cairns BA and Meyer AA. Laser resurfacing and remodeling of hypertrophic burn scars: the results of a large, prospective, before-after cohort study, with long-term follow-up. Annals of surgery 2014; 260(3): 519-532.
27. Carter CA, Jolly DG, Worden CE, Sr, Hendren DG and Kane CJ. Platelet-rich plasma gel promotes differentiation and regeneration during equine wound healing. Experimental and Molecular Pathology 2003; 74(3):244-255.
28. Xian LJ, Chowdhury SR, Bin Saim A and Idrus RB. Concentration-dependent effect of platelet-rich plasma on keratinocyte and fibroblast wound healing. Cytotherapy 2015; 17(3):293-300.
29. Heng MC. Wound healing in adult skin: aiming for perfect regeneration. Int J Dermatol 2011; 50 (2):1058-1064.
30. Eldrieny E, Sarhan N, Laag E and Badr S. Histological study of the effect of bone marrow-derived mesenchymal stem cells on healing of skin defect in adult male albino rats. Egyptian Journal of Histology 2014; 37(1):186-196.
31. Chen CC, Wang L, Plikus MV, Jiang TX, Murray PJ, Ramos R, Guerrero-Juarez CF, Hughes MW, Lee OK, Shi S, Widelitz RB, Lander AD and Chuong CM. Organ-level quorum sensing directs regeneration in hair stem cell populations. Cell 2015; 161(2):277-290.
32. Ozcelik U, Ekici Y, Bircan HY, Aydogan C, Turkoglu S, Ozen O, Moray G and Haberal M. Effect of Topical Platelet-Rich Plasma on Burn Healing After Partial-Thickness Burn Injury. Medical science monitor: International Medical Journal of Experimental and Clinical Research 2016; 22(4):1903-1909.
33. Baum CL and Arpey CJ. Normal cutaneous wound healing: Clinical correlation with cellular and molecular events. Dermatol. Surg. 2005; 31(6):674-686.
34. 34. Boothby IC, Cohen JN and Rosenblum MD. Regulatory T cells in skin injury: At the crossroads of tolerance and tissue repair. Sci Immunol. 2020; 5(47):e9631-9643.

35. Gurtner GC, Werner S, Barrandon Y, Longaker MT. Wound repair and regeneration. Nature 2008; 453 (1):314-321.

36. Rohl M, Tjernlund A, Mehta SD, Pettersson P, Bailey RC and Broliden K. Comparable mRNA expression of inflammatory markers but lower claudin-1 mRNA levels in foreskin tissue of HSV-2 seropositive versus seronegative asymptomatic Kenyan young men. BMJ Open 2015; 5(2):e006627-006631.

37. Rabello FB, Souza CD and Farina Junior JA. Update on hypertrophic scar treatment. Clinics 2014; 69 (8):565-573.

38. Yang SW, Geng ZJ, Ma K, Sun Y and Fu XB. Comparison of the histological morphology between normal skin and scar tissue. Journal of Huazhong. University of science and technology; 2016; 36(2):266-269.

39. Zhou S, Wang W, Zhou S, Zhang G, He J and Li Q. A novel model for cutaneous wound healing and scarring in the rat. Plastic and Reconstructive Surgery 2019; 143(2):468-477.

40. Fayzullin A, Ignatieva N, Zakharkina O, Tokarev M, Mudryak D, Khristidis Y, Balyasin M, Kurkov A, Churbanov S, Dyuzheva T, Timashev P. and Shekhter A. Modeling of Old Scars: Histopathological, Biochemical and Thermal Analysis of the Scar Tissue Maturation. Biology 2021; 10(2):136-143.

41. Wen X, Zheng Y, Wu J, Yue L, Wang C, Luan J, Wu Z and Wang K. In *vitro* and in *vivo* investigation of bacterial cellulose dressing containing uniform silver sulfadiazine nanoparticles for burn wound healing. Progress in Natural Science: Materials International 2015; 25(3):197-203.

42. Galko MJ and Krasnow MA. Cellular and genetic analysis of wound healing in Drosophila larvae. PLoS Biol. 2004; 2(1):e239.

43. Ramos-Lewis W, LaFever KS and Page-McCaw A. A scar-like lesion is apparent in basement membrane after wound repair in *vivo*. Matrix biology: Journal of the International Society for Matrix Biology 2018; 74(1):101-120.

44. Kim DH, Je YJ, Kim CD, Lee YH, Seo YJ, Lee JH. and Lee Y. Can platelet-rich plasma be used for skin rejuvenation? Evaluation of effects of plateletrich plasma on human dermal fibroblast. Annals of Dermatology 2011; 23(4): 424-431.

45. Younan G, Suber F, Xing W, Shi T, Kunori Y, Åbrink M, Pejler G, Schlenner SM, Rodewald HR, Moore FD and Stevens RL. The inflammatory response after an epidermal burn depends on the activities of mouse mast cell proteases 4 and 5. The Journal of Immunology 2010; 185(12):7681-7690.

46. Tanaka R, Fukushima SI, Sasaki K, Tanaka Y, Murota H, Matsumoto K, Araki T and Yasui T. In *vivo* visualization of dermal collagen fiber in skin burn by collagen-sensitive second-harmonic-generation microscopy. Journal of Biomedical Optics 2013; 18(6):061231.

47. Mahoney MG, Müller EJ and Koch PJ. Desmosomes and desmosomal cadherin function in skin and heart diseases-advancements in basic and clinical research. Dermatology Research and Practice 2010; 725647.

48. Everts P, Onishi K, Jayaram P, Lana JF and Mautner K. Platelet-Rich Plasma: New Performance Understandings and Therapeutic Considerations in 2020. International Journal of Molecular Sciences 2020; 21(20):7794-7801.

49. Lacci KM and Dardik A. Platelet-rich plasma: support for its use in wound healing. The Yale Journal of Biology and Medicine; 2010; 83(1):1-8.

50. Behm B, Babilas P, Landthaler M and Schreml S. Cytokines, chemokines and growth factors in wound healing. Journal of the European Academy of Dermatology and Venereology 2012; 26(7):812-820.

51. Guerra A, Belinha J and Jorge RN. Modelling skin wound healing angiogenesis: A review. Journal of Theoretical Biology 2018; 459(1):1-17.

52. Pettersson A, Nagy JA, Brown LF, Sundberg C, Morgan E, Jungles S, Carter R, Krieger JE, Manseau EJ, Harvey VS, Eckelhoefer IA, Feng D, Dvorak AM, Mulligan RC and Dvorak HF. Heterogeneity of the angiogenic response induced in different normal adult tissues by vascular permeability factor/vascular endothelial growth factor. Laboratory investigation; a Journal of Technical Methods and Pathology 2000; 80(1):99-115.

53. Zhang J, Nie D, Williamson K, Rocha JL, Hogan MV and Wang JH. Selectively activated PRP exerts differential effects on tendon stem/progenitor cells and tendon healing. Journal of Tissue Engineering 2019; 10(1):1-14.

54. Tonnesen MG, Feng X and Clark RA. Angiogenesis in wound healing. In Journal of Investigative Dermatology Symposium Proceedings: Elsevier 2000; 5(1):40-46.

55. Hammam MA, Antar AG, Abdou AG and Hassan RA. Angiogenesis in involved and uninvolved skin of psoriasis highlighted by cluster of differentiation 34: an immunohistochemical study. Menoufia Medical Journal 2019; 32(3):1013-1019.

56. Xu C, Wang X and Pramanik M. Imaging technologies and transdermal delivery in skin disorders. Chapter 1. Wiley- VCH. Wieinheim. Germany. 2019; pp. 1.

57. Rognoni E, Gomez C, Pisco AO, Rawlins EL, Simons BD. Watt FM and Driskell RR. Inhibition of β-catenin signalling in dermal fibroblasts enhances hair follicle regeneration during wound healing. Development (Cambridge, England) 2016; 143(14):2522-2535.

58. Gentile P and Garcovich S. Autologous activated platelet-rich plasma (AA-PRP) and non-activated (A-PRP) in hair growth: a retrospective, blinded, randomized evaluation in androgenetic alopecia Expert Opin Biol Ther. 2020; 20(3):327-337.

59. Nicoletti G, Saler M, Villani L, Rumolo A, Tresoldi MM and Faga A. Platelet rich plasma enhancement of skin regeneration in an ex-*vivo* human experimental model. Frontiers in Bioengineering and Biotechnology 2019; 7(1): 2-7.

60. Chen ZC, Wu SYS, Su WY, Lin YC, Lee YH, Wu WH, Chen CH and Wen ZH. Anti-inflammatory and burn injury wound healing properties of the shell of Haliotis diversicolor. BMC Complementary and Alternative Medicine 2016; 16(1): 487-493.

61. Nassar M, Ramadoss N, Veeran V, Paramel SM, Arul KT and Mohamed PMY. Characteristics of Collagen to Differentiate Fibrous Hyperplasia from Mesenchymal and Mixed Odontogenic tumors: A Polarized Microscopic Study. Ann Med Health Sci Res. 2017; 7(2):319-324.

62. Kim M, Kim SW, Kim H, Hwang CW, Choi JM and Kang HW. Development of a reproducible in *vivo* laser-induced scar model for wound healing study and management. Biomedical Optics Express 2019; 10(4):1965-1977.

63. Li J, Chen J and Kirsner R. Pathophysiology of acute wound healing. Clinics in Dermatology 2007; 25(1): 9-18.

64. Yildiz H, Abuaf OK, Baloglu H, Bilgili ME, Simsek HA and Dogan B. Histologic Evidence of New Collagen Formulation Using Platelet Rich Plasma in Skin Rejuvenation: A Prospective Controlled Clinical Study. Annals of Dermatology 2016; 28(6):718-724.

65. Nofal E, Helmy A, Nofal A, Alakad R and Nasr M. Platelet-rich plasma versus CROSS technique with 100% trichloroacetic acid versus combined skin needling and platelet rich plasma in the treatment of atrophic acne scars: a comparative study. Dermatologic Surgery 2014; 40(8):864-873.

66. Ibrahim ZAES, El-Tatawy RA, El-Samongy MA and Ali DAM. Comparison between the efficacy and safety of platelet-rich plasma vs. microdermabrasion in the treatment of striae distensae: clinical and histopathological study. Journal of Cosmetic Dermatology 2015; 14(4):336-346.

67. Sorg H, Tilkorn DJ, Hager S, Hauser J and Mirastschijski U. Skin Wound Healing: An Update on the Current Knowledge and Concepts. Eur Surg Res 2017; 58(1):81-94.

68. Kwan P, Hori K, Ding J and Tredget EE. Scar and contracture: biological principles. Hand Clin. 2009; 25(3):511-528.

69. Li B and Wang JH. Fibroblasts and myofibroblasts in wound healing: force generation and measurement. Journal of Tissue Viability 2011; 20(4):108-120.

70. Chellini F, Tani A, Vallone L, Nosi D, Pavan P, Bambi F, Zecchi Orlandini S and Sassoli C. Platelet-rich plasma prevents in *vitro* transforming growth factor-β1-induced fibroblast to myofibroblast transition: involvement of vascular endothelial growth factor (VEGF)-A/VEGF receptor-1-mediated signaling. Cells 2018; 7(9):142-150.

71. Erdag G, Qureshi HS, Patterson JW and Wick MR. CD34-positive dendritic cells disappear from scars but are increased in pericicatricial tissue. Journal of Cutaneous Pathology 2008; 35(8):752-756.

72. Limandja GC, Belien JM, Scheper RJ, Niessen FB and Gibbs S. Hypertrophic and keloid scars fail to progress from the CD34- /α-smooth muscle actin (α-SMA)+ immature scar phenotype and show gradient differences in α-SMA and p16 expression. Br J Dermatol. 2020; 182(4):974-986.

73. Raj D, Brash DE and Grossman D. Keratinocyte apoptosis in epidermal development and disease. J. Invest. Dermatol. 2006;126(1):243-257.

الملخص العربى

دراسة هستولوجية للتأثير العلاجى المحتمل للبلازما الغنية بالصفائح الدموية على إلتآم الحرق الجلدي من الدرجة الثانية ومنع تكون الندبات في ذكر الجرذ الأبيض البالغ

أسماء محمد منصور، منى تيسير صادق،عصام محمود لعج، ابتسام فؤاد عكاشه، جيهان محمد سليمان

قسم الأنسجة وبيولوجيا الخلية، كلية الطب، جامعة طنطا، مصر

المقدمة: يعتبر الحرق اصابة جلدية تتسبب فى تكوين ندبات ضخامية. تمثل البلازما الغنية بالصفائح الدموية وسيلة علاجية تستخدم فى التام الجروح.

الهدف من العمل: دراسة التأثير العلاجي المحتمل للبلازما الغنية بالصفائح الدموية على التئام حروق الجلد من الدرجة الثانية و تكون الندبات الناتجه عنه.

المواد والطرق: أجريت هذه الدراسة على ٧٠ من ذكور الجرذان البيضاء تم تقسيمهم عشوائياً إلى ثلاث مجموعات رئيسية؛ المجموعة الأولى والثانية والثالثة. تضمنت المجموعة الأولى ٣٠ جرذًا تم تقسيمهم عشوائيًا إلى ثلاث مجموعات فرعية متساوية؛ المجموعة الفرعية ١-أ (لجمع الدم)، المجموعة الفرعية ١- ب (المجموعة الضابطة، تم الاحتفاظ بها دون أن تتلقى أى علاج) والمجموعة الفرعية ١- ج (المجموعة الضابطة، والتى تلقت حقنة واحدة تحت الجلد من البلازما الغنية بالصفائح الدموية، ثم تم الحصول على عينات الجلد بعد أسبوع واحد و بعد أربعة أسابيع). تضمنت المجموعة الثانية ٢٠ جرذاً تم فيهم إحداث حرق من الدرجة الثانية بواسطة قضيب معدني مسخن ثم تم تقسيمهم إلى مجموعتين فرعيتين متساويتين: المجموعة الفرعية ٢-أ (تم فحصها بعد أسبوع واحد) والمجموعة الفرعية ٢- ب (تم فحصها بعد أربعة أسابيع). إشتملت المجموعة الثالثة على ٢٠ جرذاً تم فيهم إحداث حرق من الدرجة الثانية ثم تم علاج الفئران موضعيا على الفور بحقنة واحدة تحت الجلد تحتوى على ٠,٤ مل من البلازما الغنية بالصفائح الدموية، وتم تقسيمهم إلى مجموعتين فرعيتين متساويتين: المجموعة الفرعية ٣-أ (تم فحصها بعد أسبوع واحد) والمجموعة الفرعية ٣- ب (تم فحصها بعد أربعة أسابيع). تم فحص المقاطع باستخدام المجهر الضوئي (بعد صباغتها بصبغتا الهيماتوكسيلين والأيوسين، صبغة التلويدين الأزرق، صبغة مالوري ثلاثية الكروم بالإضافة إلى الصبغات المناعيه للكشف عن أكتين العضلة الملساء α و سي دي ٣٤) وكذلك فحصها بالمجهر الإلكتروني. أجريت الدراسة القياسية والتحليل الإحصائي لمتوسط سمك البشرة ومتوسط النسبة المئوية لمساحة الكولاجين ومتوسط كثافة لون التفاعل المناعى ل أكتين العضلة الملساء α و سي دي ٣٤.

النتائج: بالمقارنة مع المجموعتين الفرعيتين الغير معالجتين٢أ و ٢ب، أظهرت كلتا المجموعتين المعالجتين ٣أ و ٣ ب التئاما افضل ونضج أسرع للندبات والتى كانت أكثر وضوحا بعد أربع أسابيع من حقن للبلازما الغنية بالصفائح الدموية.

الاستنتاج: ان البلازما الغنية بالصفائح الدموية ذات تأثير فعال على التئام حروق الجلد من الدرجة الثانية و نضج الندبات الناتجة عنها.